3D Basin-scale groundwater flow modeling as a tool for geothermal exploration: Application to the Geneva basin, Switzerland-France

Marion Alcanié, Marine Collignon, Olav Møyner, Matteo Lupi

3D Basin-scale groundwater flow modeling as a tool for geothermal exploration: Application to the Geneva basin, Switzerland-France

Marion Alcanié[1], Marine Collignon[1], Olav Møyner[2], Matteo Lupi[1]

[1]Department of Earth Sciences, University of Geneva, Geneva, Switzerland
[2]SINTEF Digital, Oslo, Norway.

Key Points:

- We perform 14 basin-scale simulations to investigate how thermal and petrophysical properties, and tectonic features affect fluid flow.
- We propose a conceptual model showing that fluid flow is driven by gravitional flow following preferential fault pathways.
- We propose an integrated methodology in MRST that could be used for the assessment of geothermal resources in sedimentary basins.

Corresponding author: M. Alcanié, `marion.alcanie@unige.ch`

Corresponding author: M. Lupi, `matteo.lupi@unige.ch`

Abstract

Switzerland promotes the energy transition by supporting the development of geothermal energy. We built a 3D basin-scale fluid flow model of the Geneva Basin, France-Switzerland, using the open-source Matlab Reservoir Simulation Toolbox (MRST). The model is calibrated on available well and active seismic data.

The goal of the numerical study is to investigate temperature and pressure distribution at depth that could be used to identify large-scale positive thermal anomalies. Previous and ongoing projects have assessed the geothermal potential of the region using static conductive models interpolated from bottom hole temperatures. However, a consistent basin-scale fluid flow model of the Geneva Basin is still lacking. We perform 14 numerical models, articulated into three complementary studies to investigate how thermal properties, petrophysical parameters and tectonic features affect fluid flow. We constrain our simulations by implementing a progressive degree of geological and petrophysical realism to study the physical processes driving fluid flow in the Geneva basin.

We propose based on the simulation results a conceptual model showing that fluid flow is driven by the down-welling of meteoric waters that cool down rocks at the edge of the Geneva Basin. In turn, this temperature drop promotes the up-welling of warmer fluids in the centre of the basin where we suggest that exploration for geothermal resources should focus. Finally, the approach presented in this study could be used for the first assessment of geothermal resources in other sedimentary basins.

1 Introduction

Changes in precipitation rates and the accelerating melting of glaciers due to global warming will strongly affect groundwater resources, whose demand is already expected to increase for the upcoming decades due to demographic growth and urbanization (Mays, 2013). Moreover, these resources may be subject to anthropogenic contamination during well activities (Dragon, 2008; Jasechko et al., 2017). Surface- and groundwater is not only crucial for the development of our society (Velis et al., 2017) but can also play a key role in mitigating the effect of climate change through the development of renewable energies, such as hydropower and geothermal energy (Jialing et al., 2015).

Despite their elevated energy potential, high-enthalpy geothermal systems remain under-developed and confined in volcanic areas. In contrast, the development of low- to medium-enthalpy geothermal systems increased significantly over the last decades in suburban regions where the energy needs are the highest (Breede et al., 2013; Olasolo et al., 2016). Additionally, several examples have shown that the energy from medium-enthalpy geothermal systems represents a valuable asset for the reduction of green-house gas emissions, while supporting our growing economy (Kulcar et al., 2008; Nowak, 2011; Glassley, 2014). For instance, the Paris basin has been exploited since 1969 (Housse & Maget, 1976; Lopez et al., 2010) and it is estimated that about $7{\times}10^9$ MWh may be recovered from groundwater stored in the Dogger aquifer (Lavigne & Maget, 1977; Menjoz et al., 2004; Hamm & Treil, 2013). Similarly, heat is produced in Southern Germany to support the city of Munich (Böhm et al., 2013). More recently, (Taillefer et al., 2018) investigated crustal fluid flow pointing out the importance of topographic effects in deep-reaching crustal circulation. Luijendijk et al. (2020) have shown that thermal springs in the Alps are fed by meteoric water circulating impacting groundwater composition.

Following the Paris' agreement Switzerland is planning to reduce CO_2 emissions by, among other initiatives, promoting the development of geothermal resources via several scientific and industrial programs. In this framework, the Canton of Geneva is exploring geothermal opportunities in the Greater Geneva Basin (GGB, Figure 1) (Faessler et al., 2015) thanks to the *GEothermie2020* [1] program. Preliminary results have been encouraging (Carrier et al., 2019) and numerical models have already been used to evaluate the feasibility of

[1] https://www.geothermie2020.ch

heat storage in the Molasse and Malm formations of the GGB (Collignon et al., 2020). However, basin-scale fluid flow processes remain poorly documented in the region. This is particularly relevant when planning a sustainable exploitation of geo-energy resources in urbanized areas, for fifty years or more (Sweetkind et al., 2010). Besides wells and hydrogeological data, heat and mass transport numerical models may provide key information about groundwater temperature at depth (Person et al., 1996).

Various codes (e.g. FEFLOW (Trefry & Muffels, 2007; Diersch, 2013), CSMP++ (Matthai et al., 2007; Coumou et al., 2008), HYDROTHERM (Kipp et al., 2008), TOUGH2 (Pruess et al., 2012) among several others) have been developed over the years for the simulation and quantification of fluid flow processes in the upper crust. While most of these codes grant state-of-the-art numerical solutions, they suffer from limitations. Possible limitations of these codes are their restrictive accessibility (e.g. commercial software), the complex structure and syntax of the simulators and/or the lack of internal support for complex grid geometries. To overcome these aspects, we use the Matlab Reservoir Simulation Toolbox (MRST) (Lie, 2019; Krogstad et al., 2015). Matlab is widely used and allows the rapid implementation of an integrated workflow. MRST is a set of libraries initially conceived for the simulation of oil and gas reservoirs and related applications (e.g. carbon capture storage). MRST offers flexible and complex gridding capabilities, easy integration of wells and efficient solvers. In addition, a geothermal module was recently implemented and tested by Collignon et al. (2020) to investigate low- to medium-enthalpy hydrothermal and groundwater systems (*MRST geothermal module* [2]).

A second shortcoming of basin-scale numerical models is the often limited degree of geological realism due to sparse datasets or even a lack of subsurface data. In the GGB (Figure 1), a wealth of geological and geophysical data data have been compiled in the framework of the GeoMol project that assessed the subsurface potentials of the Alpine Foreland Basins (Molasse basins) across Europe for a sustainable planning and use of natural resources (The GeoMol Team, 2015; Allenbach et al., 2017). The shallow aquifers of the GGB have been investigated for almost 80 yrs (Joukowsky, 1941). It led to the development of several static conductive geological models investigating temperatures at depth (Allenbach et al., 2017; Chelle-Michou et al., 2017). These models, however, did not account for advective flow and to date, a dynamic groundwater flow model of the region is still missing. We present here the first 3D basin-scale groundwater flow model of the GGB and investigate the physical processes driving fluid flow at depth. Our results allow the identification of potential regions that are suitable for geothermal prospecting for hydrothermal reservoirs.

The manuscript is structured as follows. We first introduce the geological setting and the numerical model illustrating the organisation of the simulations. We then present the results of our initial model and its improvements that progressively increase the degree of geological realism throughout our simulations. We then propose a final model and discuss its impact for the development of geothermal energy in the GGB. Finally, we discuss the limitations of our study and its wider implications.

2 Geological setting of the Great Geneva Basin

The GGB spans over a Swiss-French transnational zone located at the southwestern edge of the North Alpine foreland basin (Signer & Gorin, 1995), also called Molasse Basin, which extends parallel to the Alps from France to Austria (Figure 1a). The Molasse Basin formed during the Alpine orogeny as a result of the collision between the European and the African plates (Trümpy, 1980; Homewood et al., 1986; Burkhard & Sommaruga, 1998). The structural setting of the basin is characterized by two major sets of faults (thrusts and strike slip faults) (Figures 1, and 3) (Sommaruga, 1997, 1999; Charollais et al., 2013). The GGB extends over nearly 2200 km^2 from about the city of Nyon in Switzerland until Annecy in France. It is bounded in the South

[2] https://www.sintef.no/projectweb/mrst/modules/#geothermal

and North by the thrusting fronts of the Alps and the Jura Mountains, respectively (Figure 1). Thrust systems have been mapped in both the Alps and the Jura and show an overall NE-SW strike across the GGB. Late orogenic activity resulted in low relief flexures (NE-striking) such as the Salève mountain (Figure 1). Strike slip faults develop syn- and post-thrusting mostly during Oligocene, offsetting the low-angle structures. These lateral faults are linked to counter-clockwise rotation driven by the micro Apulian plate and are characterized by NW-SE strikes (Gorin et al., 1993; Dupuy, 2006; Paolacci, 2012; Charollais et al., 2013). The Geneva Basin is considered as a sub-basin of the GGB.

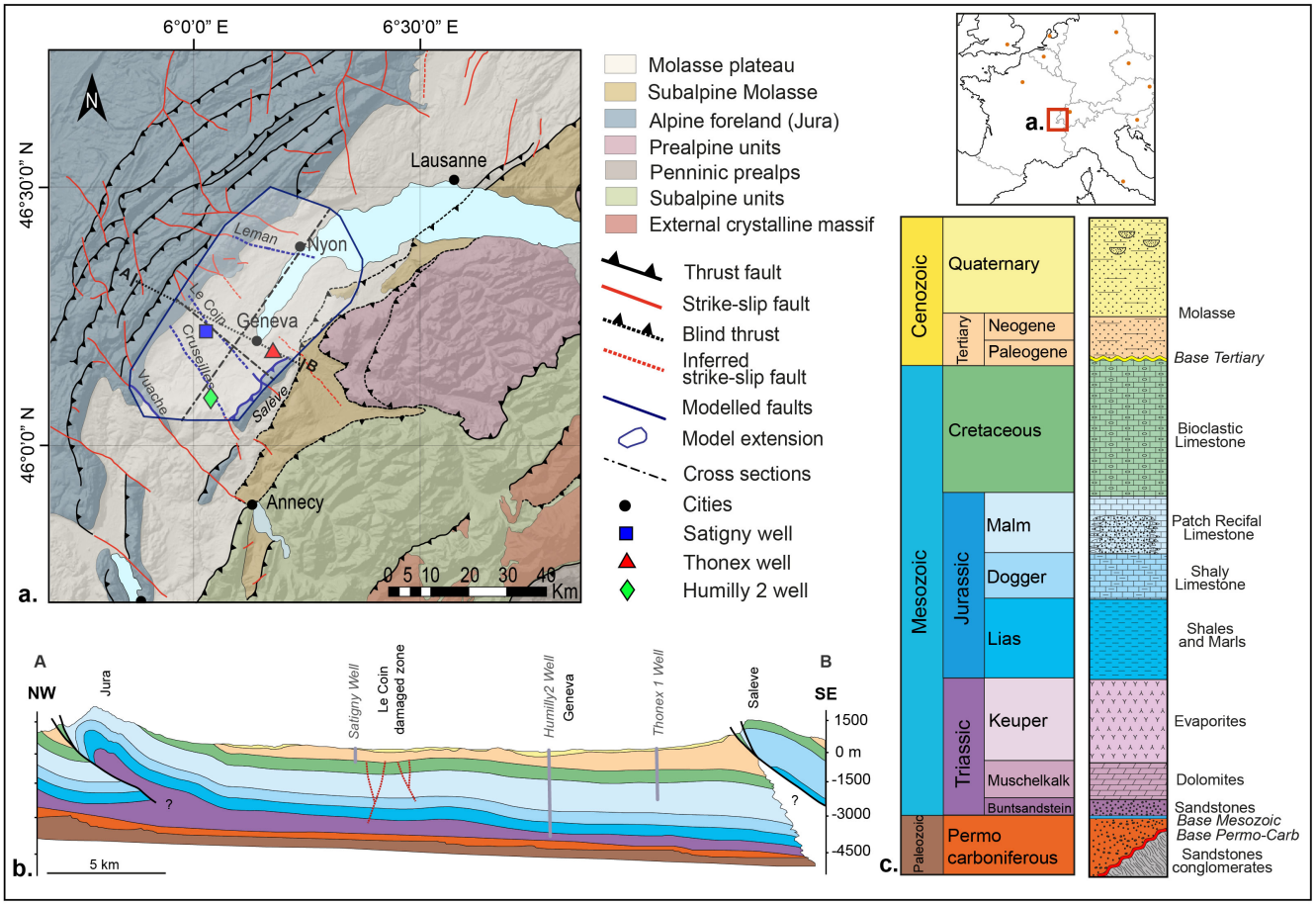

Figure 1. Geology and tectonic setting of the Great Geneva Basin. a. Regional simplified structural map of the Great Geneva Basin showing the extent of the model (thick blue line) and the location of the main faults and deep wells (geometric symbols) used as control points. The black dashed line A-B shows the location of the cross section in panel **b.** (modified after (Signer & Gorin, 1995). **c.** Simplified lithostratigraphic log of the sedimentary cover of the Great Geneva Basin. Note that the faults crossing the basin have been simplified. Interpreted well data are extracted from Capar et al. (2015); Rusillon (2017) and **a.**, **b.**, **c.** are modified after Rusillon (2017). Interpreted seismic lines are obtained from Clerc et al. (2015); Allenbach et al. (2017).

The GGB is composed of a thick Mesozoic and Cenozoic sedimentary sequence deposited over a Variscan crystalline basement, which dips towards SE (Signer & Gorin, 1995; Paolacci, 2012). We review, from bottom to top, the units composing the GGB pointing out their reservoir potential for the exploitation of hydrothermal resources. The sedimentary cover, from permo-carboniferous to Quaternary (Figure 1b, c), is well-described in the literature (Ramsay, 1963; Charollais et al., 2007; Sommaruga et al., 2012). Suitable aquifers for the exploitation of hydrothermal resources occur in porous sandstones, karstified limestones (not considered in our model), reef or peri-reefal deposits, or dolomitized limestones (Paolacci, 2012; Rusillon, 2017; Makhloufi et al., 2018). The Permo-carboniferous clastic sediments have been suggested to be at about 4500 m depth (Signer & Gorin, 1995). They are linked to the Variscan orogeny and they fill up confined grabens that could be optimal aquifers (porous sandstones after Rusillon2017, but still poorly documented). The Triassic is characterized by shallow marine deposits, composed (from lower to upper units) of sandstones, dolomites, and evaporites. Dolomites are suggested to be a possibly exploitable reservoir for hydrothermal uses, with porosities up to $\sim$15%. However, permeabilities have been estimated to be low (2.1×10^{-17} m^2) (Rusillon, 2017). The Lower Jurassic sediments are made of marls and shales, progressively evolving towards carbonates and some local reefs in the Middle and Upper Jurassic. Oolithic Dogger limestones present a porosity up to $\sim$8% and permeabilities of about 7×10^{-16} m^2 with high heterogeneities (Rusillon, 2017), permeability values varying up to four orders of magnitudes due to lateral facies variations in this unit that coincides with lateral thickness variations. Pre-recifal Malm deposits show a $\sim$5% porosity and a permeability of about 1×10^{-16} m^2 (Rusillon, 2017). During the Lower Cretaceous, the depositional environment was a shallow-water carbonate platform with bioclastic limestones (Rusillon, 2017). The uppermost part of the Lower Cretaceous is marked by an erosive and highly karstified surface and this unit, when found, is considered as a potentially promising reservoir (Rusillon, 2017). The Upper Cretaceous is missing in the sequence. The Mesozoic is overlaid by siliciclastic deposits from Oligocene to late Miocene, thinning out towards the foothills of the Jura. The Molasse deposits are locally characterized by high porosity and permeability of about 20% and 5×10^{-14} m^2, respectively (Rusillon, 2017; The GeoMol Team, 2015). Yet, the Molasse is an extremely heterogeneous reservoir, permeability values varying up to five orders of magnitudes in sandstone patchy non-connected bodies.

The region was initially prospected for hydrocarbon resources (Moscariello, 2019), and therefore, the geology of the basin has been extensively studied (Signer & Gorin, 1995; Charollais et al., 2007; Gorin et al., 1993; Rybach, 1992). A review of the historical well catalog compiling available stratigraphic data can be found in Rusillon (2017) and Brentini (2018). From the thousands of wells drilled in the GGB, ca. forty wells are fully documented. They contain logs and cores information, such as porosity and permeability. Additionally, data may list fluid state (i.e. liquid/gas), flow rate, salinity, and bottom hole temperatures. Fifteen wells are located in the modeled volume, but only three of them were drilled down to the Cretaceous or deeper (i.e. Thonex, Satigny, and Humilly2, reaching 2530 m, 677 m and 3051 m depth, respectively, Figure 1). Only the well Humilly2 reaches the top of Permo-carboniferous unit. Several 2D seismic lines were also acquired in the framework of the *GEothermie2020* program for a total of 1500 km (Sommaruga et al., 2012). More recently, the large amount of data acquired during the 60ties and 70ties have been reprocessed. Tectonic features such as fault geometry are extracted from seismic lines (Clerc et al., 2015) and their interpretation is still in progress. Bottom hole temperatures have been corrected in the framework of ongoing geothermal exploration (Chelle-Michou et al., 2017). New gravity and geoelectric data (Guglielmetti et al., 2020; Carrier et al., 2019, 2020) as well as passive seismic methods (Planès et al., 2020; Antunes et al., 2020) provided further constrains for the modeling part. These wells and geophysical measurements allowed the definition of the local geothermal gradient after correction of temperatures measured at numerous wells drilled in the GGB (Chelle-Michou et al., 2017).

3 Numerical model and geological information

3.1 Numerical tool

We investigate groundwater flow in the Geneva Basin using the *geothermal* module of MRST (Collignon et al., 2020). We consider a single-phase H_2O compressible Darcy flow. The system of coupled nonlinear partial differential equations describing the conservation of mass and energy in three dimensions is solved using a finite volume method. The nonlinear system of equations is solved with Newton's method, where the Jacobians are efficiently and accurately computed by automatic differentiation. The geothermal module also provides the necessary equations of state to account for density and viscosity changes. Further details about the geothermal module can be found in Collignon et al. (2020).

We have made a few assumptions to simplify the numerical simulations and to allow an affordable computation time. We account for single-phase pure water because the salinity values measured in the GGB are on average less than 10 g/L (Rusillon, 2017), which would have little effect on the water density and viscosity (Spivey et al., 2004). Such salinity values are too low to significantly affect the enthalpy and energy calculations (Driesner, 2007) and the pressure and temperature conditions in the upper crust of the GGB are below boiling curve (Rybach, 1992; Chelle-Michou et al., 2017). In the model they are set as hydrostatic pressure and constant geothermal gradient according to Chelle-Michou et al. (2017). The fluid density and viscosity is computed following the Spivey et al. (2004) formulation, implemented by default in the geothermal module of MRST (Collignon et al., 2020). Thermal fluid parameters are chosen in the range of appropriate literature values (Sharqawy, 2013). Thermal conductivity and specific heat capacity of fluid are set constant at 0.6 $W \cdot m^{-1} \cdot K^{-1}$ and 4182 $J.kg^{-1}.K^{-1}$, respectively, as they do not significantly vary in the range of the investigated pressures and temperatures (Driesner, 2007).

We do not account for mechanical deformation in our model. This assumption is supported by the very low deformation rate recorded in the GGB (Antunes et al., 2020). Geochemical processes, such as water-rock interaction are also neglected. Finally, we assume that the petrophysical (Table 1) and hydraulic properties, as well as the basal heat flux, are constant in time.

3.2 Hierarchy of the simulations

We investigate with numerical simulations the physical and petrophysical parameters that may affect fluid flow and temperature distributions at depth. Our hypothesis is that fluid transport in the Geneva Basin is affected by topography (Taillefer et al., 2018) and by faulted zones, which provide a preferential pathways for fluid in an overall low-permeability basin, see (Table 1). Our goal is to propose a conceptual model of fluid flow for the Geneva Basin that could be used to identify regions promising for geothermal exploitation. To tackle this problem, we first design an initial model (*Model 0*, see Figure 2) that serves as a reference model and a comparison for the other simulations.

We then propose three sets of investigations (summarized in Figure 2), focusing on three independent aspects. The thermal study looks at the effects of the geothermal gradient and basal heat flux derived from Chelle-Michou et al. (2017), for a total of nine simulations and allows us to select the most complete thermal conditions for the Geneva Basin. The petrophysical study, testing porosity and permeability distributions, contains three different case scenarii derived from Allenbach et al. (2017) and Rusillon (2017). Testing different petrophysical scenarii also allows us to reduce the uncertainties due to the measurement methods. The third set of simulations investigates how basin-scale fault systems may affect temperature distributions in the basin. We successively investigated the permeabilities and porosities of these fault systems. In total the 14 simulations that we run for this scope allowed us to select the most accurate parameters to build the *Final Model*.

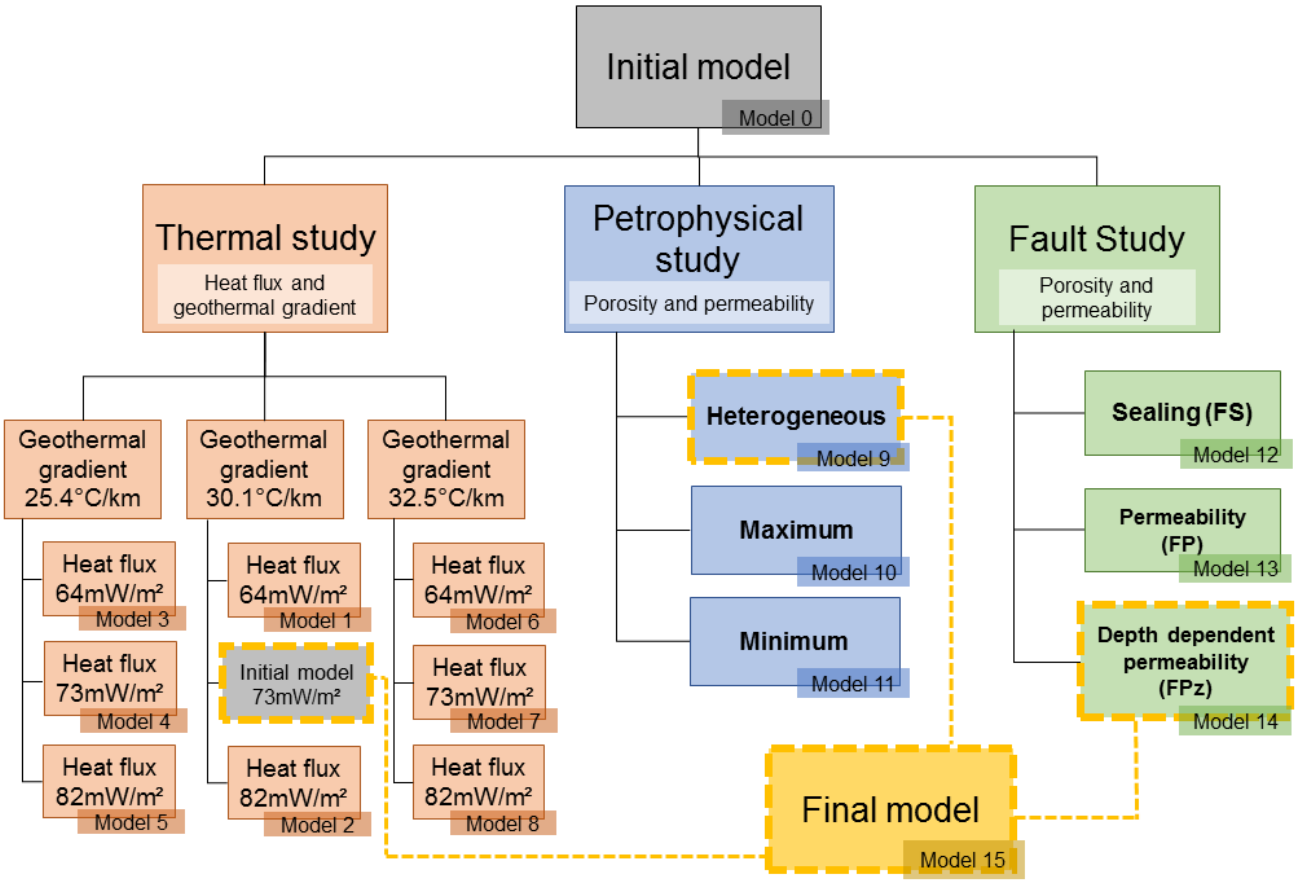

Figure 2. Workflow of this study. We start from an initial model and separately test the effects of heat flux and geothermal gradient (*Thermal study*), petrophysical properties (*Petrophysical study*) and the effects of faults (*Fault study*). The thick dashed yellow lines represents the parameters selected for *Final Model*. The details and parameters of the simulations can be found in the supplementary material. Time and grid resolution chosen for the models have been tested to ensure the robustness of our resolution and do not present any aliasing effects.

3.3 Model design

Our 3D geological model is derived from Allenbach et al. (2017) and considers nine lithostratigraphic units that have been previously described by Capar et al. (2015); Clerc et al. (2015) and summarized in the stratigraphic log of Figure 3. The units are divided by lithostratigraphic horizons interpolated in the 3D Geomol static model (Clerc et al., 2015; Allenbach et al., 2017). In addition to the stratigraphic horizons, we also consider the topography of the Geneva Basin (Figure 4). Each lithostratigraphic unit presents morphological variations as the horizons are not parallel to each other, being obtained by interpolating 2D active seismic profiles. The 3D geological model is about 40 km by 35 km in the x- and y-directions, respectively (Figure 3).

The maximum elevation is about 1600 m in the Jura Mountains, while the maximum depth is 5500 m at the foothills of the Alps.

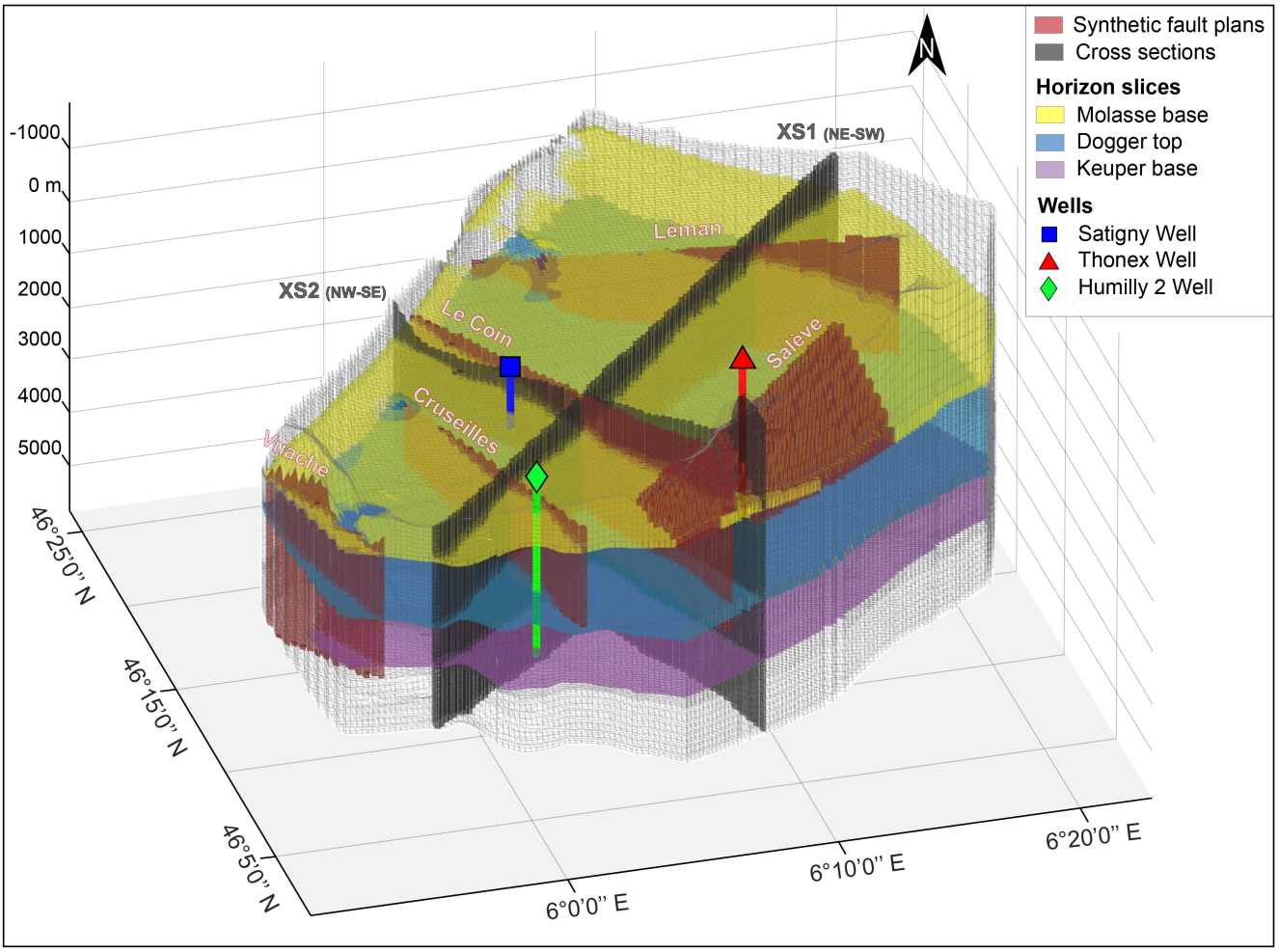

Figure 3. 3D geometric model of the Great Geneva Basin. Locations of wells, faults and cross-sections used in this study are represented in the model of the Geneva Basin. Modified from Planès et al. (2020); Antunes et al. (2020); Carrier et al. (2020)

.

The meshing was done with MRST using a corner point geometry that is then converted into the unstructured MRST format. For each layer, a constant number of cells is specified in the vertical direction and elevation is corrected in case of overlapping points. The grid has a total of about 250000 active cells. Each cell is about 483x418 m, in the x- and y- direction, respectively. Along the z axis, we allow the cells thickness to vary depending on the thickness of the unit and the amount of cells with the corner point geometry definition. A

finer grid resolution was used for the final model, with about 322x278 m, in the x- and y-direction respectively for a total of about 500000 cells.

Faults are added to the model in the third set of simulations (*Fault study*, Figure 2). In MRST, faults are by default considered as surface planes or discontinuities and not as objects, which implies that we cannot assign petrophysical properties, such as porosity and permeability, at the cell centres but through the faces using transmissibility multipliers (Lie, 2019; Nilsen et al., 2012). We thus create high-aspect ratio structured objects representing damage zones with negligible offset rather than fault planes that is consistent with Clerc et al. (2015). For practicality in this study we will use the terms faults and damage zones interchangeably. Our 3D model did not allow us to include a degree of geological realism that would allow accounting for all the faults mapped in the Geneva Basin, as it would result in excessively high computational costs. Therefore, the poorly documented, shallow faults across Quaternary units only and with small offset are not taken into account. Four strike slip faults and one major thrust fault are considered in the model. They represent the most prominent fault complexes offsetting the GGB (Clerc et al., 2015) and were selected as they reach the Mesozoic units unlike the smaller scale, faults offsetting the Quaternary that we choose to exclude for computational reasons. All the faults implemented in our models match the fault model used by Chelle-Michou et al. (2017) and Dupuy (2006). The Salève thrust and the Vuache strike slip fault have both been observed cropping out at the surface (Charollais et al., 2013). The surface expressions of these five tectonic structures are shown in Figures 1 and 3, and correspond to faults identified by previous authors (Allenbach et al., 2017; Chelle-Michou et al., 2017; Dupuy, 2006; Eruteya et al., 2019).

3.4 Initial and boundary conditions

For the three studies, the total simulation time is 500 kyrs with prescribed time-steps of 500 yrs in all models. The final model is simulated for over 1 Myr with time-steps of 250 yrs. The first time steps are smaller to ensure convergence of the solver. We prescribe an initial hydro-static pressure field in the model using the following relationship: $P = \rho_w \ g \ z_{corrected}$, where ρ_w is the water density and g the gravity constant. Here, $z_{corrected}$ is not the absolute coordinate of the model but instead the thickness of the water column taken from the model surface, and has thus been corrected with respect to the elevation of the model topography. The initial temperature field is defined using a constant geothermal gradient of 30 °C/Km and a surface temperature, T_{surf}, of 10 °C, for the initial model (*Model 0*), following the first geothermal gradient scenario proposed by Chelle-Michou et al. (2017). In the *Thermal study*, geothermal gradients of 25 and 33 °C/Km are also investigated in association with a different heat flux (Figure 2, see supplementary material for values).

We prescribe no-flow conditions on the lateral and bottom boundaries. The lateral boundaries are also thermally insulated. As our simulations span over more than 100kyrs, we are not modeling yearly oscillations, such as seasonal recharge or precipitation variations, which are not captured by our model time steps. Similarly, we do not consider mass flow coming in or out of the model because of lack of measurements. The Geneva lake was not modeled because of the absence of data regarding water infiltration. We also simplified the model by not taking into account any free water bodies, such as the Rhone river and the Lake Geneva. The top boundary is characterized by a Dirichlet condition, with a constant pressure and temperature (T_{surf}) of 1 atm and 10 °C, respectively. This temperature corresponds to the average annual temperature in the region (Chelle-Michou et al., 2017). The bottom boundary has a Neumann condition, characterized by a spatially constant basal heat flux. Depending on the investigated thermal setup (see Thermal study in Figure 2), this value is set from 64 to 82 $mW.m^{-2}$ (Commission Suisse de Géophysique, 1995; Chelle-Michou et al., 2017).

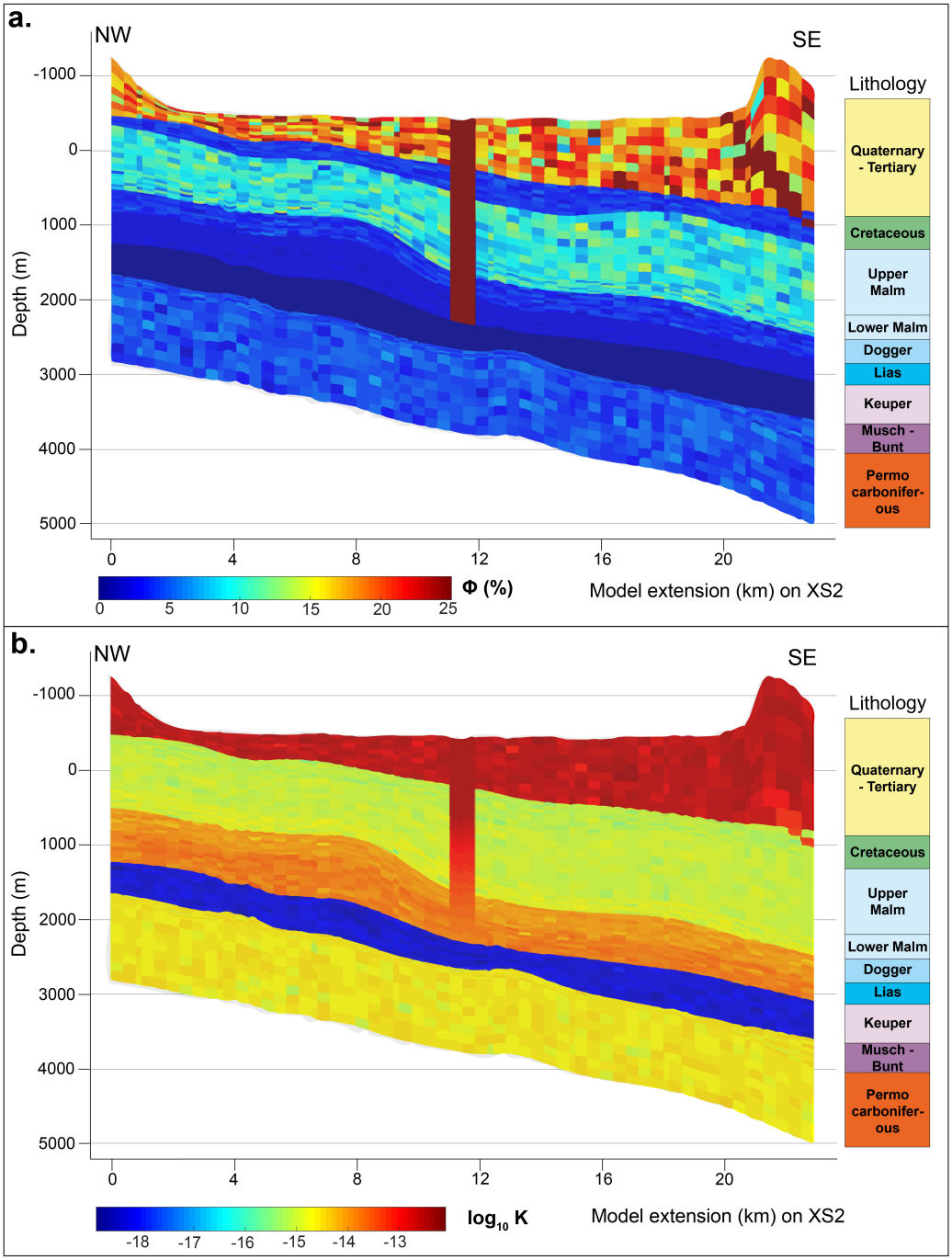

Figure 4. Petrophysical model for the *Heterogeneous* and *Final* model, i.e. model (9). Porosity (**a.**) and permeability (**b.**) distribution shown on the NW-SE vertical cross section (XS2 in Figures 1 and 3). Values are derived from The GeoMol Team (2015). The Salève thrust and Le Coin strike slip fault are also cross-cut by this section in the *Final Model*. The modeled geological sequence is shown in Figure 1. Permeability and porosity distributions for both *Permeable* and *Impermeable* models can be found in the Supplementary Material.

Table 1. petrophysical parameters of the *Model 0*. μ is the arithmetic average and σ the standard deviation

Modeled lithology	**Porosity**		**Permeability**		**Density**	**Thermal Conductivity**	**Specific Heat Capacity**
Units	**%**		**m^2**		**kg.m^{-3}**	**W · m^{-1} · K^{-1}**	**J.kg^{-1}.K^{-1}**
	μ	σ	μ	σ			
Quaternary Tertiary	10.7	4.80	6.5×10^{-14}	1.3×10^{-13}	2400	2.6	1140
Cretaceous	1.5	0.83	7.1×10^{-16}	6.2×10^{-16}	2670	3.0	928
Upper Malm	4.3	3.37	2.6×10^{-16}	2.7×10^{-16}	2690	2.8	1021
Lower Malm	2.6	2.33	2.0×10^{-16}	3.3×10^{-16}	2740	2.6	967
Dogger	2.8	0.85	8.2×10^{-16}	1.3×10^{-15}	2650	2.8	972
Lias	2.3	0.58	7.2×10^{-16}	1.5×10^{-14}	2640	2.6	935
Keuper	0.1	0.01	9.9×10^{-19}	9.9×10^{-16}	2840	2.6	887
Muschelkalk Buntsandstein	3.3	2.80	1.4×10^{-15}	2.1×10^{-15}	2740	2.9	923
Permo Carboniferous	3.3	2.80	1.4×10^{-15}	2.1×10^{-15}	2710	2.9	887

3.5 Petrophysical model

The petrophysical parameters characterizing the investigated models were obtained from the wells spread across the GGB (Rusillon, 2017). The location of the three wells, Thonex, Satigny and Humilly2, used as control points in this study, is shown in Figure 3. The reference model, *Model 0*, considers a simplified geometry and laterally homogeneous petrophysical parameters. Petrophysical properties are characterised in our models by permeability, porosity, rock density, thermal conductivity and specific heat capacity. They are defined for each geological unit. Only permeability and porosity are changed between simulations, the other parameters being fixed. Each lithostratigraphic unit of *Model 0* has constant and isotropic properties (Table 1), which represent arithmetic average values of the compiled literature (i.e. (Rusillon, 2017; Capar et al., 2015)). The karstified features represent a small portion of our model. They are approximated as a porous medium at large scale due to lack of morphometric data of the fractures (e.g. width and length) to characterize an equivalent porous media model. When available from the literature, a range of values (minimum, maximum, arithmetic average and standard deviation) for each parameters is given in the Supplementary Material. Thermal conductivities are taken from measured samples (Rusillon, 2017), and if not available for a given unit, we consider the value measured for a similar lithology outside the Geneva Basin (Chelle-Michou et al., 2017). A single value is often given in the literature without further details. The specific heat capacity of each unit is extracted from Waples and Waples (2004) and Schärli and Rybach (2001). The models investigated in the thermal study have the same petrophysical properties as in *Model 0*.

In the petrophysical study, we then consider the effect of permeability and porosity variations with respect to *Model 0*. The investigated setups are summarized in Figure 2. We first test two models with the maximum (*Permeable Model*) and minimum (*Impermeable Model*) permeability and porosity values measured from the GGB well samples for each geological unit. The petrophysical properties remain constant for each layer in both models. We then investigate a variable model (*Heterogeneous Model* in Figure 2), where permeability and porosity varies within the same geological unit. We generate random real-value assuming a Gaussian distribution, reproducing measurement errors. More specifically, the permeability and porosity vary as a Gaussian variable generated with Matlab comprised between the maximum and the minimum measured values (Capar et al., 2015), (Figure 4). The available standard deviations for each unit are listed in Table 1 and reflect the large variability and scarcity of permeability data.

Petrophysical parameters are again modified along the fault geometry for the fault study (Figure 2). We consider whether the permeability of the faults in the GGB is high (*Permeable Fault Model*), low (*Sealing Fault Model*) or depth-dependant (*Depth-varying Permeable Fault Model*), where faults have a depth-varying permeability, according to log(K) = -11.5 – 3.2*log(z) (Manning & Ingebritsen, 1999; Ingebritsen & Manning, 2010), if z > 1. K is the permeability in m^2 and z the depth in km. For the first kilometer we set a fixed permeability values as logarithmic depth values between 0 and 1 yield large deviations from what has been measured in the GGB. Permeability values across the Tertiary - Quaternary layer were measured on core samples in the laboratory (Rusillon, 2017; Allenbach et al., 2017). They display a large heterogeneity, ranging from 10^{-17} to 10^{-12} m^2. Manning and Ingebritsen (1999) derived a depth dependent law for the whole continental crust (> 30 km). However, in our study we only focus on the first 5 km of the sedimentary filling of the basin. We thus tuned the permeability value in the first kilometer, by taking the average of the maximum measurements obtained from Rusillon (2017) and Allenbach et al. (2017). We find a permeability of 3×10^{-13} m^2 for the first kilometer.

Ultimately, the *Final Model* represents the geologically more complex model and considers a Gaussian distribution of the permeability and porosity, similarly to the *Heterogeneous Model* and has, in addition to it, faults with a depth-varying permeability as in the *Depth-varying Permeable Fault Model*.

4 Results

The three studies allow us to understand how the geothermal gradient and geological heterogeneities affect temperature distributions at depth.

4.1 Description of *Model 0*

Steady-state is reached in less than 100 yrs for the pressure at the control points (Figure 5). The equilibrium pressure field shows negligible variation from the initially prescribed hydrostatic pressures. The temperature evolution is slower and presents a global increase. Steady-state is reached around 400 kyrs.

Figure 6a shows the temporal evolution of the temperature in the Geneva Basin at the Top of the Dogger unit. At the beginning of the simulation the Upper Dogger records temperatures of about 50°C and 120°C to the NW and SE, respectively. After 100 kyrs we notice an increase of temperature in the center of the basin and a cooling below the topographic highs (NW and SE). Throughout the simulation, temperature increases in the center of the basin, while the domains in the NW and SE become progressively colder, when compared to the initial state. After 500 kyrs the temperature in the center of the basin is higher than 120 °C. The thermal evolution observed in *Model 0* corresponds to a re-equilibrium between heat flux and geothermal gradient. Only the Satigny control point (blue square) shows about 20 °C more than what it was measured at about 600 m depth (Carrier et al., 2019). The cross sections in Figure 6b suggest that the isotherms (initially following

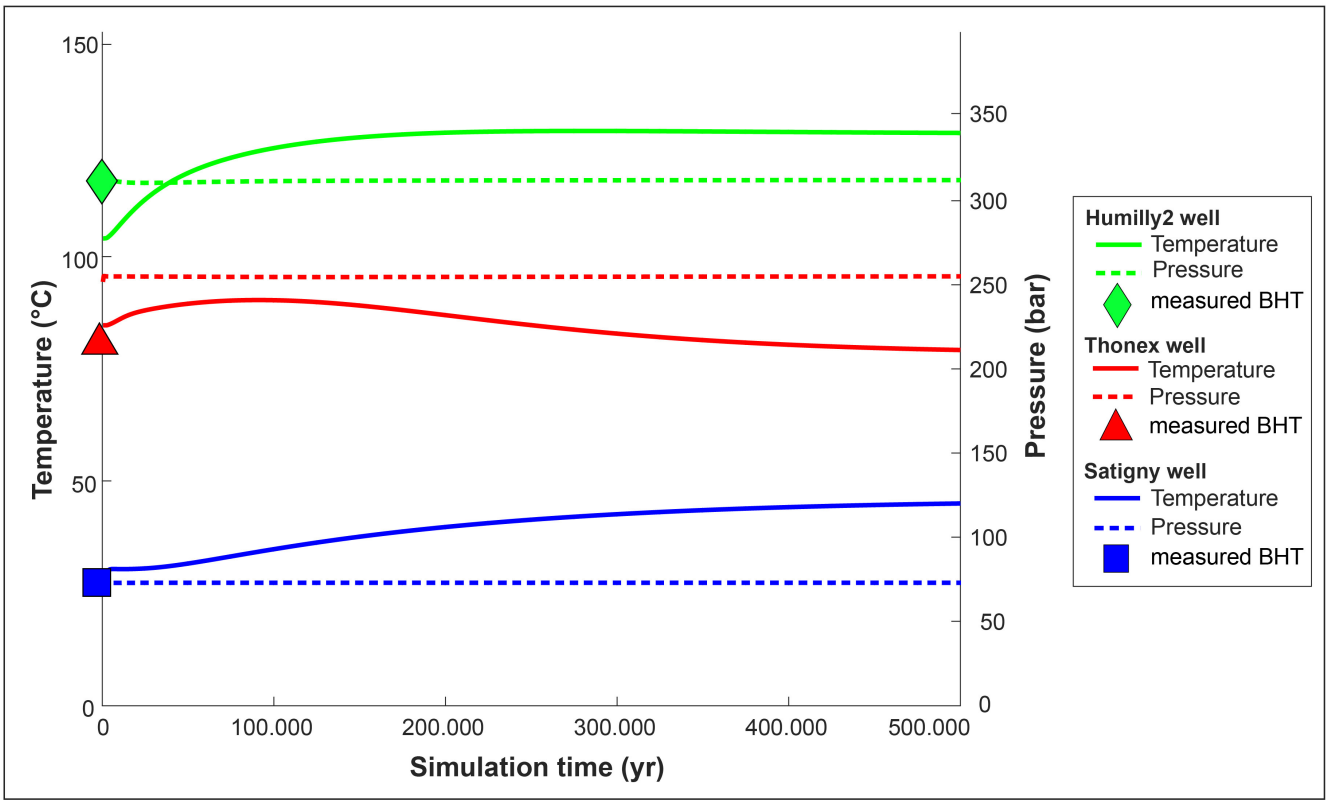

Figure 5. Temporal Evolution of *Model 0* at control points. Pressure (bar) and temperature (°C) are given at the three monitoring wells for *Model 0*. Well location is shown in Figures 1, 3.

the SE-dipping of the geological units) bulge in the center of the Geneva Basin after about 200 kyrs. In this region, weak convection cells develop due to advection of warmer fluids, while below the topographic highs cold groundwater is down-welling causing a deflection of the isotherms.

4.2 Effect of the geothermal gradient and heat flow

This first set of simulations investigates the effects of the basal heat flux and initial geothermal gradient on the temperature distribution in the Geneva Basin (Figure 7). Results are presented as temperature anomalies with respect to *Model 0*.

Our results show that the impact of the heat flux on the final temperature distribution is more pronounced than the impact of the geothermal gradient by one order of magnitude. Temperature variations up to 40 °C are observed when varying the basal heat flux, whereas changing the temperature gradient yields to variations of only 4°C at most. The geothermal gradient has an impact only in the early stages of the simulations. Interestingly, the central portion of the Geneva Basin is more prominently affected by heat flux variations than other parts of the basin. This effect is possibly due to topographic effects driving percolation of shallow

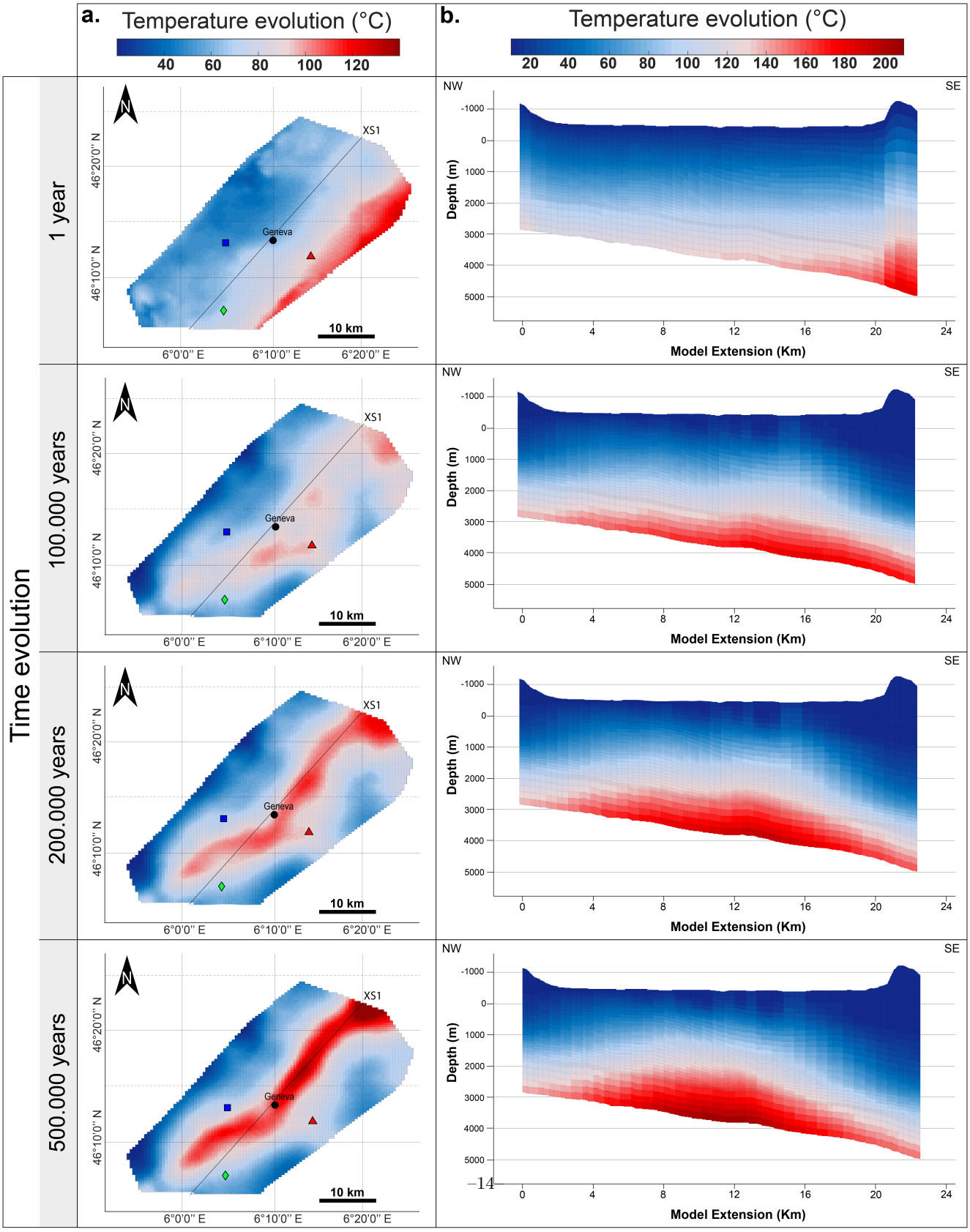

Figure 6. Temporal Evolution of the temperature for *Model 0* recorded at **a.** the top of the Dogger horizon and **b.** along XS2 (location on Figure 3) for 500 simulated kyrs. Red triangle, blue square and green diamond: wells monitored in Figure 5 with location and penetration depths shown in Figure 1.

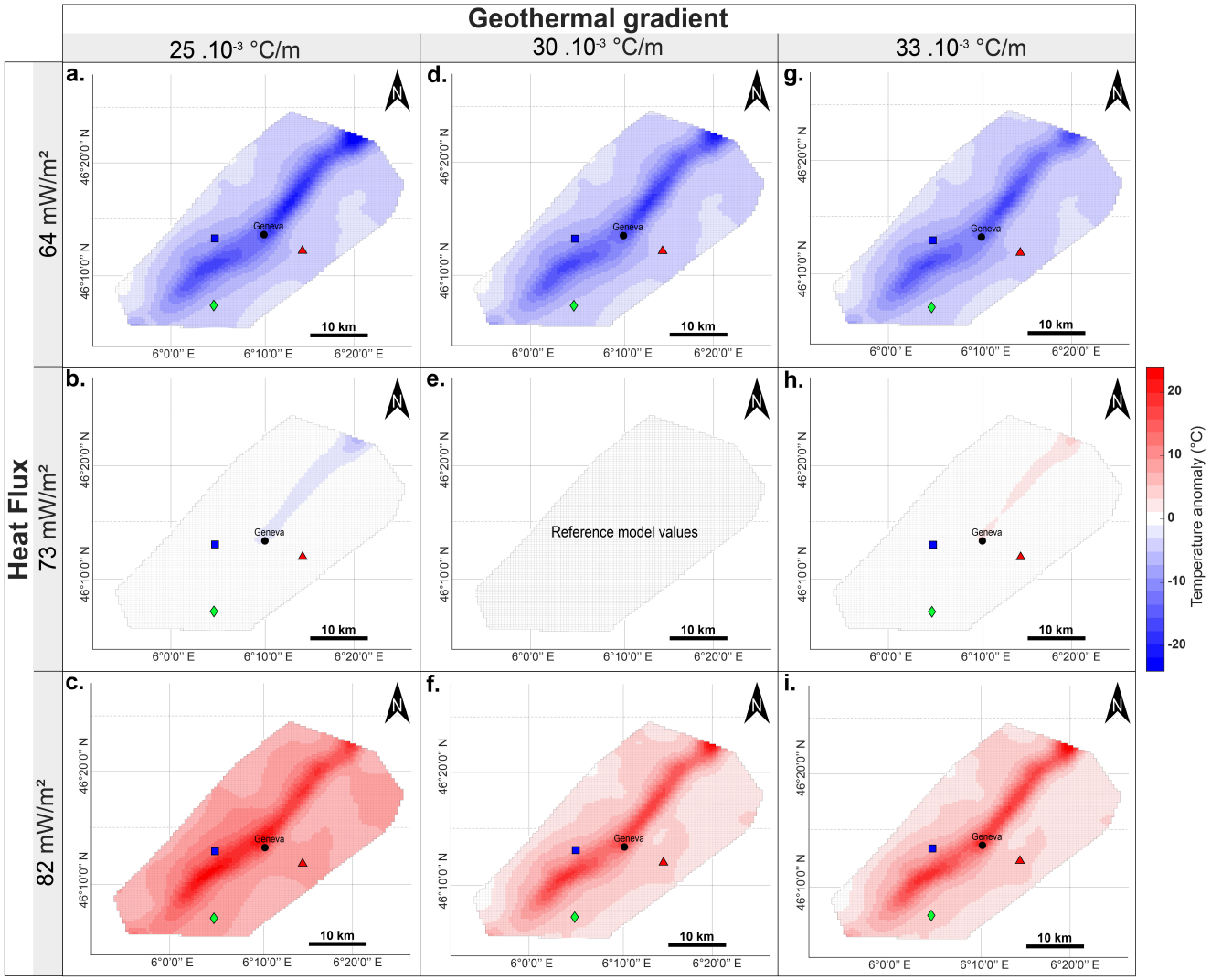

Figure 7. Thermal study. Impact of the geothermal gradient (horizontal) and heat flux (vertical) on the temperature anomalies recorded at the Dogger top after 500 kyrs. Temperature anomalies are computed with respect to *Model 0* ($\Delta T = T_{model} - T_{model0}$). Red triangle, blue square and green diamond: wells monitored in Figure 5 with location and penetration depths shown in Figure 1. Model parameters are given in supplementary material.

waters and ultimately fluid flow at depth. The most extreme values are found below Lake Geneva in the upper northern part of the basin.

4.3 Effects of the petrophysical heterogeneities

We also investigate the impact of porosity and permeability on the temperature distribution in the Geneva Basin (Figure 8). Petrophysical values used for the three investigated scenarios are listed in the supplementary material. Results are presented as temperature anomalies with respect to *Model 0*. Generally, petrophysical parameters have a stronger impact on the temperature distribution than the heat flux values investigated previously (see Figure 8 compared to Figure 7). The temperature variations show also higher amplitudes for the petrophysical study than the thermal study (Figures 7– 8). When investigated separately, permeability has a stronger impact on temperature distribution than porosity.

The *Heterogeneous Model* (Figure 8a, b, c) behaves more like the *Permeable Model* (Figure 8d, e, f) with higher porosities and permeabilities than the *Impermeable Model* (Figure 8g, h, i). For *Heterogeneous* and *Permeable Models*, a global temperature decrease is observed, and the central feature (i.e. temperature bulge) is no longer clearly visible. Lower permeability/porosity values (Figure 8a, d, b, e, c, f) have a stronger impact on the model behavior than higher values. When looking at the temperature distribution, the steady state is also reached faster than for *Model 0*, whereas the *Impermeable Model* does not reach the steady-state after 500 kyrs. Larger temperature anomalies are observed in the *Impermeable Model* with a cooling down in the model center and below Lake Geneva compared to *Model 0*, as well as a warming up along the model sides, in the south-east and north-west. Due to very low permeability values, advection is hindered and temperature equilibrium is not achieved. Lower permeability/porosity values (Figure 8a, d, b, e, c, f) result in an increase of the overall model temperature.

Temperature anomalies are generally lower at the base of the Keuper (up to -40°C) than at the Base of the Molasse (-5 to -10 °C) for both the *Heterogenous Model* and *Permeable Model*, suggesting that the global cooling of the system increases with depth. The focusing feature in the center is visible in all simulations (Figure 8a, d, g), suggesting a strong topographic control in the shallow part of the model that vanishes at depth.

4.4 Effect of the faults

The relative impact of structural heterogeneities on pressure and temperature distribution is shown by introducing fault systems. Three models with different permeabilities of the damage zones are presented, namely: *Sealing Fault Model (FS)*, *Permeable Fault Model (FP)* and *Depth-varying Permeable Fault Model (FPZ)*. Temperature and pressure are compared to the first time step (1 year) because the static initial model is no longer the same than *Model 0* once fault structures have been added. The anomalies are reported in Figure 9. Darcy velocities are also reported for each model.

Darcy velocities, and thus flow rates are proportional to the magnitude of the permeabilities (Figure 9a, b, c). Thermal convection cells occur in the shallow part of the Molasse layer, in each model, showing down-welling and up-welling flow. They are, however, bypassed with the presence of permeable faults, which show high Darcy velocities (in the order of 20 to 30 cm/yr). Almost no flow occurs in the Keuper (between 2000 and 3000 m depth), which also records the lowest permeabilities. The flow rates in the Dogger are increased compared to *Model 0* thanks to the presence of permeable faults. Regions of the Malm have heterogeneous flow rates where intersecting the fault structures. The pressure distribution shows little variation over 500 kyrs (2 bars in the Malm), which is consistent with the results of *Model 0* (Figure 6. A small pressure drop, starting from the bottom of the model, is visible for the sealing fault model (Figure 9d). When adding permeable faults (Figure 9e, f), a slightly over-pressured layer appears in proximity of the Keuper compared to the previous simulations.

The temperature increases with time for the three fault models. For the model shown in Figure 9g, faults have a small impact on the resulting temperature distribution, which is similar to the one of *Model 0* at the

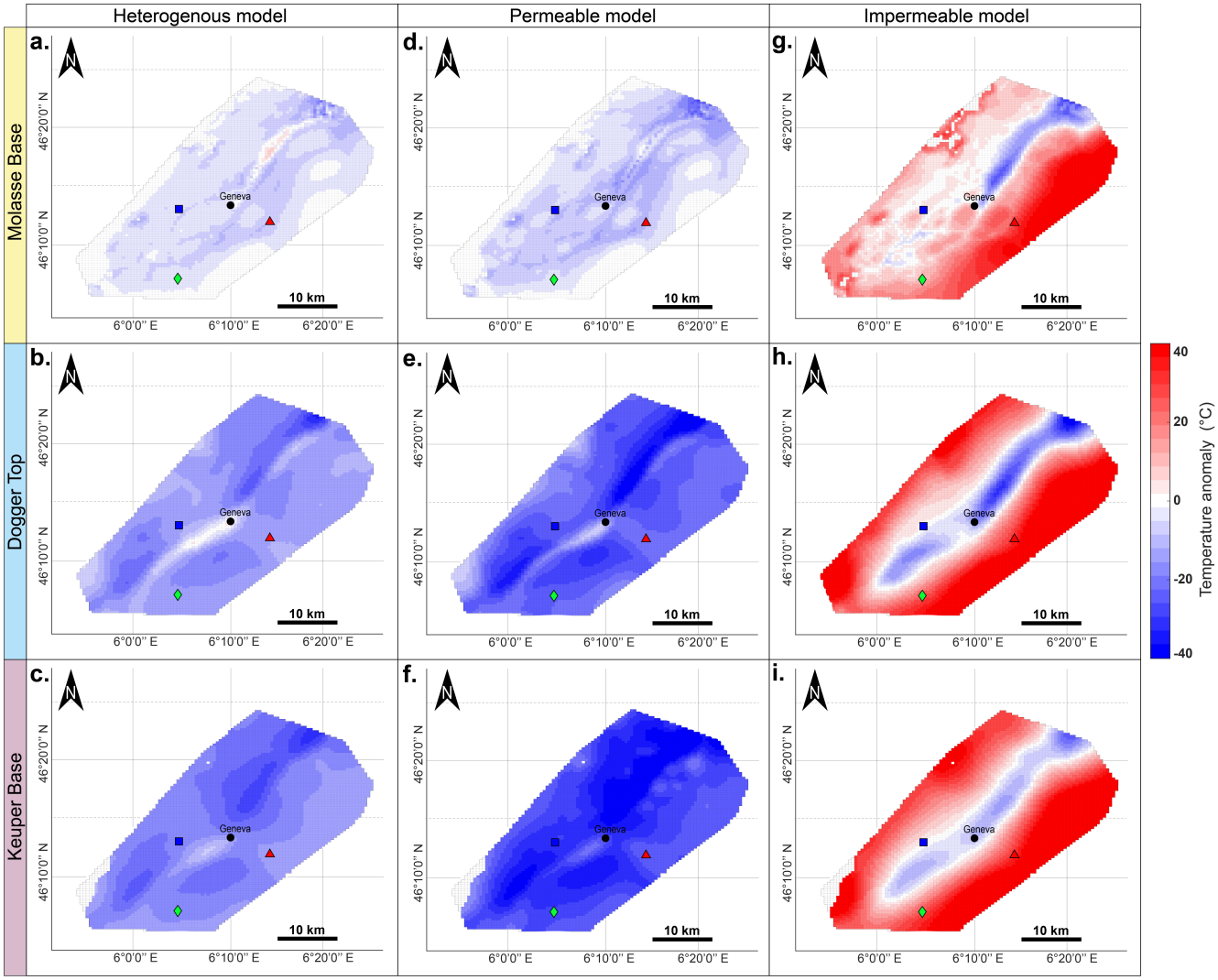

Figure 8. Petrophysical study. Impact of petrophysical variations on the temperature anomalies with respect to *Model 0* (Δ T = T_{petro} – T_0), recorded after 500 simulated kyrs for the *heterogeneous model* (**a.**, **b.**, **c.**), the *maximum* model (**d.**, **e.**, **f.**) and the *minimum* model (**g.**, **h.**, **i.**), taken at three different stratigraphic levels ("Molasse Base", "Dogger Top" and "Keuper Base", see Figure 3). Red triangle, blue square and green diamond: wells monitored in Figure 5 with location and penetration depths shown in Figure 1. Model parameters are described in the supplementary material.

same simulated time. With permeable faults (Figure 9h, i), their location is highlighted in the distribution of the temperature anomalies, with sometimes high contrasting values between two neighboring cells (e.g. Figure 9h).

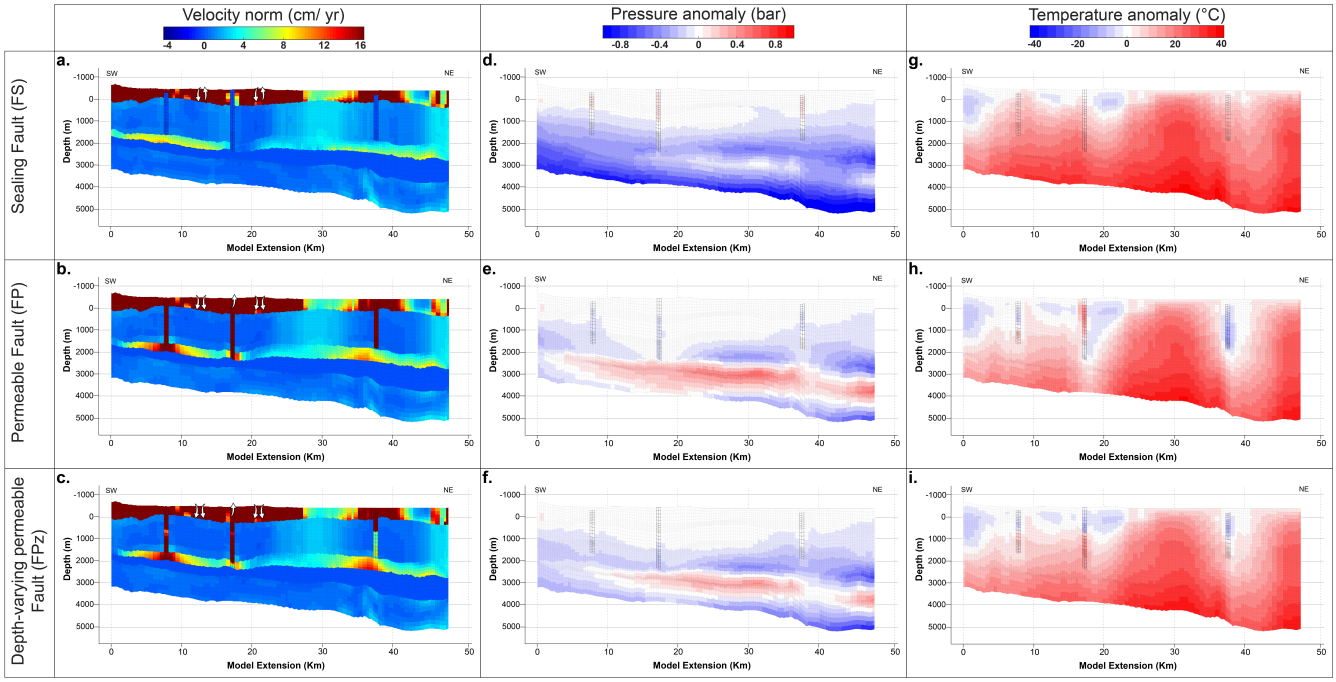

Figure 9. Effects of the faults on the model. Impact of different fault permeabilities on the Darcy velocity norm (**a.**, **b.**, **c.**), pressure anomalies (**d.**, **e.**, **f.**) and temperature anomalies (**g.**, **h.**, **i.**), recorded along XS1 (Location Figure 3). XS1 cross-cuts three strike slip faults: "Léman", "le Coin" and "Cruseilles". Three permeability scenarios are considered: 1) sealed fault (top), permeable fault (middle) and depth-varying permeable fault (bottom). Pressure and temperature anomalies are computed with respect to the first time step of the simulation ($\Delta T = T_{fault(500.000)} - T_{fault(1)}$ and $\Delta P = P_{fault(500.000)} - P_{fault(1)}$). Velocity norm is the scalar value calculated from the norm of the 3-component vector *velocity* in each cell of the model. Parameter values are given in the supplementary material.

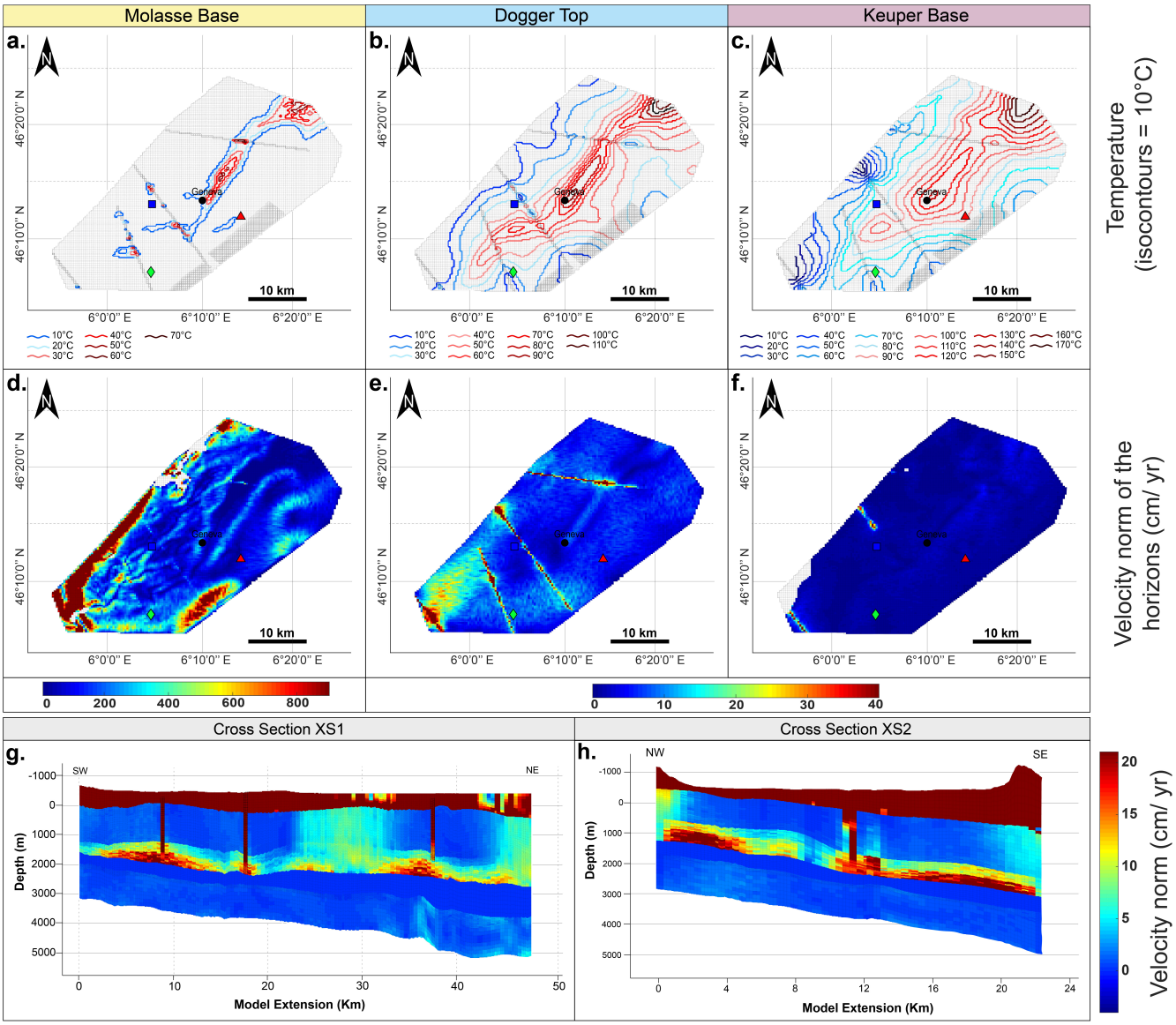

Figure 10. Final Model. Temperature (**a,b,c**) and velocity norm (**d,e,f**) distribution after 500 simulated kyrs at three stratigraphic levels of the final model: Molasse Base (left), Dogger Top (middle) and Keuper (right). (**g,h**) Velocity norm along the cross-sections XS1 and XS2, respectively. Red triangle, blue square and green diamond show the locations of the wells monitored in Figure 5 with location and penetration depths shown in Figure 1. Velocity norm is the scalar value calculated from the norm of the 3-component vector *velocity* in each cell of the model. Velocity vector plot for this model can be found in Supplementary Material. Model parameters are described in the supplementary material.

4.5 Final Model

In the previous sets of simulations the petrophysical, thermal and structural parameters are investigated separately to evaluate their relative influence on the pressure and temperature distributions in the Geneva Basin. However, all these processes have a strong impact and should be considered together in the final proposed model for the Geneva Basin. Therefore, we compile for each of our three sets of simulations the best-case scenario and propose a *Final Model*, which we suggest is the most geologically complete model for the Geneva Basin.

A similar temperature distribution, with a central bulge as observed in *Model 0*, is visible in the *Final model*. This feature is perturbed by the main faults (Figure 10a, b, c). A temperature decrease over the whole model is mainly caused by the petrophysical heterogeneities (Shemin Ge & Garven, 1992; Guillou-Frottier et al., 2013). In the vicinity of the faults, rapid changes in temperature distributions can be observed especially in shallow regions (Figure 10a). Even if the central part of the basin still shows the warmest temperatures, the shape of the plume is highly affected by the faults. Tectonic structures are indeed known to create preferential pathways and local hydrothermal areas, where fluid can move very quickly (Sibson, 1996; Person et al., 1996), (Figure 10e). Even if the thermal field is mostly controlled by heat conduction in sedimentary basins (Przybycin, 2015), temperature distribution can also contribute to fuel and promote advective circulation (Figure 10d, e, f). With an increase of temperature, fluid density decreases and limit conditions are possibly reached when thermal convection can start (Bitzer & Carmona, 2001; Przybycin, 2015), (Figure 10d, e, g, h).

In our final model, the presence of strike-slip faults in the Dogger permeable layer contributes to the development of convection (Figure 10g, h). Geothermal anomalies may also be strongly affected by fluid flow in high permeability layers (Garibaldi et al., 2010; Guillou-Frottier et al., 2013). We observe this effect in particular in the Tertiary and Quaternary units in association with thermal convection (Figure 10d). The flow rates in this layer can be extremely high, with values up to 10 m/yr. An example in the Geneva Basin is the recently drilled Geo-01 Satigny well (Figure 10). The fluid in the permeable damaged zone is warmer than the surroundings, and artesian flow and temperature anomalies were recorded (Carrier et al., 2019). Below the Keuper the flow velocity decreases (Figure 10f) and both the topography and fault influence are drastically reduced.

5 Discussion

5.1 Comparison with previous studies in the Geneva Basin

To define the final model we considered the average heat flux of 73 $mW.m^{-2}$ given by Commission Suisse de Géophysique (1995). We keep a linear geothermal gradient of 30 °C/Km. These values represent the best average case for the GGB, based on previous simulations where we observe little variations in the temperature distribution, even when testing different geothermal gradients. For the petrophysical values, the most geologically representative model is the *Heterogeneous Model*, as it accounts for lateral permeability and porosity variations. It also represents an arithmetic average of the petrophysical values measured for the GGB (Rusillon, 2017). For high permeability values, topography driven advection is enhanced, and therefore warmer fluids up-well more efficiently, while colder shallow fluids down-well, cooling down the deeper units of the basin. Faults are believed to show variable permeability in this area (Cardello et al., 2017). Additionally, Ingebritsen and Manning (2010) consider the effect of compaction in most fault zones, consistent with a permeable fault scenario decreasing with depth. Hence the most geologically relevant model is the *FPz model* that should be integrated to the *Final Model*. Moreover, the most complete geological model broadly agrees with corrected bottom hole temperature data at the wells (see Supplementary Material Figures).

The geophysical data acquired in the Geneva Basin have been collected for the prospection of hydrocarbon resources (Moscariello, 2019). This intense exploration allowed the development of thermal studies of the GGB that assessed the geothermal state of the basin providing temperature maps at various depths (Chelle-Michou

et al., 2017; Capar et al., 2015). Such studies consider the entire Molasse foreland basin and propose thus a thermal model at a larger regional scale than our study. Consequently, some variations from these studies are observed in our results, although they overall remain in good agreement. For instance, Chelle-Michou et al. (2017) propose for the GGB a slightly negative temperature anomaly at the base of the Salève ridge that is also visible in our simulations and identified as well by Capar et al. (2015). However, Chelle-Michou et al. (2017) shows a positive thermal anomaly near the Humilly2 well, which we do not observe in our simulations. This anomaly is probably due to local geological structures that we do not fully consider in our model for computational reasons. The distribution of the isotherms shown by Capar et al. (2015) highlights that the 70°C isotherm mainly follows the topography and occurs at about 2000 m depth in the center of the basin, which is consistent with our results. Our simulations show that the 140°C isotherm may be encountered at about 3100 m depth in the centre of the basin, which is 10°C to 20°C higher than Capar et al. (2015).

5.2 Limitations of the assumptions

We argue that the geological realism of our 3D basin-scale model try to represent the state-of-the-art knowledge of the Geneva Basin. Using a depth-dependent geothermal gradient based on proposed scenario from Chelle-Michou et al. (2017) would also further constrain the model temperature distribution. Some assumptions, such as considering damage zones rather than fault planes are reasonable considering the regional-scale of our model. Including additional Quaternary faults in our model could lead to the development of sub-surface local convection cells. However, these latter would have a negligible impact on the basin-scale flow. Other processes, such as seasonal recharge variations or infiltration from free water bodies would affect the flow and heat exchange in the subsurface. However, these processes play at different temporal and spatial scale than our study. We would recommend to investigate these effects at a smaller temporal scale and focusing on the subsurface layer to reduce the high heteorgeneities uncertainties once infiltration rates have been constrained by isotopic data. Uncertainties in the petrophysical and thermal parameters are mostly due to the chosen interpolation and measurements methods. The petrophysical heterogeneities in our model could be better constrained using an appropriate kriging method. However, a reliable kriging would require having a statistically sufficient number of samples, which is currently not the case for the deeper stratigraphic units of the basin. Including these refinements into the model and calibrating the results with well tests would help producing more constrained maps of thermal anomalies.

When comparing our results with the temperatures measured at wells there are discrepancies that are intrinsically related to the concept of numerical modeling. Numerical models, our included, make several simplifications that cause the difference between the measured (T_{BHT}) and modeled (T_{mod}) temperatures. For instance, the differences shown in Figure 5 (and for the *Final Model* in Supplementary Material) at the control points may be linked to the fact that *Model 0* does not consider the complex heterogeneity that characterizes a sedimentary basin. In addition, we used an initial constant geothermal gradient that does not consider possible local anomalies. Overall differences between our model and previous static models become more pronounced towards greater depths, where the number of deep-reaching wells is limited and may bias the accuracy of static interpolated models. The three deep wells (i.e. deeper than 3000 m) drilled in the Geneva Basin are probably not sufficient to be able to fully assess a conclusive comparison between real and numerical data. Subsurface dynamic data and geochemical tracers may help to validate or disprove our conceptual model. The model output parameters we can compare to field data are temperature, pressure and velocity. Unfortunately, only temperatures can be calibrated based on measured data. The lack of geochemical data limits the constrain of the flow velocities and pressure information are not available for the region. Three wells cannot provide a statistically significant comparison to conclude on the best representation of the Geneva Basin thermal state. Neverthless, we argue that we are proposing the most complete model integrating the available knowledge on

geological complexity. We can also argue that increasing the overall model complexity would in turn increase the uncertainties of the model predictions as well.

5.3 Implications and applications

The methodology developed in this study has been carried on entirely inside MRST that allows affordable, easy to handle and rapid prototyping of hydrothermal simulations. For instance after model set up, the *Final Model* was computed in approximately five days without HPC for half a million cells model. The flexibility in MRST also allows efficient model set up. This is useful to test a large range of parameters simultaneously and check the best variable set, which is what is encountered in geothermal reservoir modeling. Giving a fast proof of concept translates into providing a decision-making tool at low cost for further actors of the field. We believe that the approach introduced in this study may represent a first tool to assess the basin scale groundwater flow of a region that is prospected for hydrothermal resources (Andersson, 2007; Baujard et al., 2007). Understanding regional-scale groundwater flow is also necessary to better implement and develop sites for the storage of heat and reduce the risk associated to pollution of groundwaters (Dragon, 2008).

Most of basin-scale studies of fluid flow developed over the last three decades mainly investigated 2D numerical models (Homewood et al., 1986; Shemin Ge & Garven, 1992; Bitzer & Carmona, 2001; Lupi et al., 2010). 3D regional models were developed more recently, thanks to the increase of available computational power and parallelization. These focused on the thermal state of the basins (Duddy et al., 1994; Bonté et al., 2018) or on hydromechanical processes taking place at depth (Hairuo Qing & Mountjoy, 1992; Montegrossi et al., 2018). However, only a few studies investigated 3D Darcy flow coupled with thermal processes, (Przybycin et al., 2017; Guillou-Frottier et al., 2020). Compared to conductive static models of the GGB (e.g. Chelle-Michou et al. (2017)) that do not account for advective flow, our simulations show a different picture. While static conductive models (Chelle-Michou et al., 2017) show sub-horizontal isotherms, our study shows instead that cold fluids percolate from topographic heights driven by higher hydraulic heads (Figure 11) where the isotherms bulge in the middle of the basin. The circulation cools down the regions below the topographic highs, while promoting the up-welling of warmer fluids in the center of the basin. The corollary is that geothermal exploration targeting hydrothermal fluids shall concentrate in the center of the basin instead of at its edges. Our final model suggests that strike slip faults may be suitable locations for fluid-drive thermal anomalies. However, Antunes et al. (2020) suggest that these fault may be active or easily reactivated due to the current orientations of the main stress tensors driving tectonic deformation in Western Switzerland. Therefore, geothermal exploration, including injection/production, may comport some risks. For this reason, a suitable alternative target for geothermal exploration may be the buried thrusts identified in the centre of the basin by seismic prospection (Allenbach et al., 2017).

Figure 11 highlights that the evaporites, typically characterised by low permeability and porosity, segregates horizontally the basin into two distinct flow regimes. Above the evaporites, the flow is dominated by advection of cold fluids, while below the Keuper conduction governs the heat transport (and possibly very limited advection). The evaporites act as a barrier, preventing the deeper lithostratigraphic units to be cooled by the shallower percolating fluids. The mixing between shallow and deep fluids is therefore only possible in selected regions, i.e. along faults crossing deep and shallow units. A last advective flow regime, characterised by sometimes high velocity, is observed in the vicinity of the faults that act as preferential flow pathways (Figure 10 and 11).

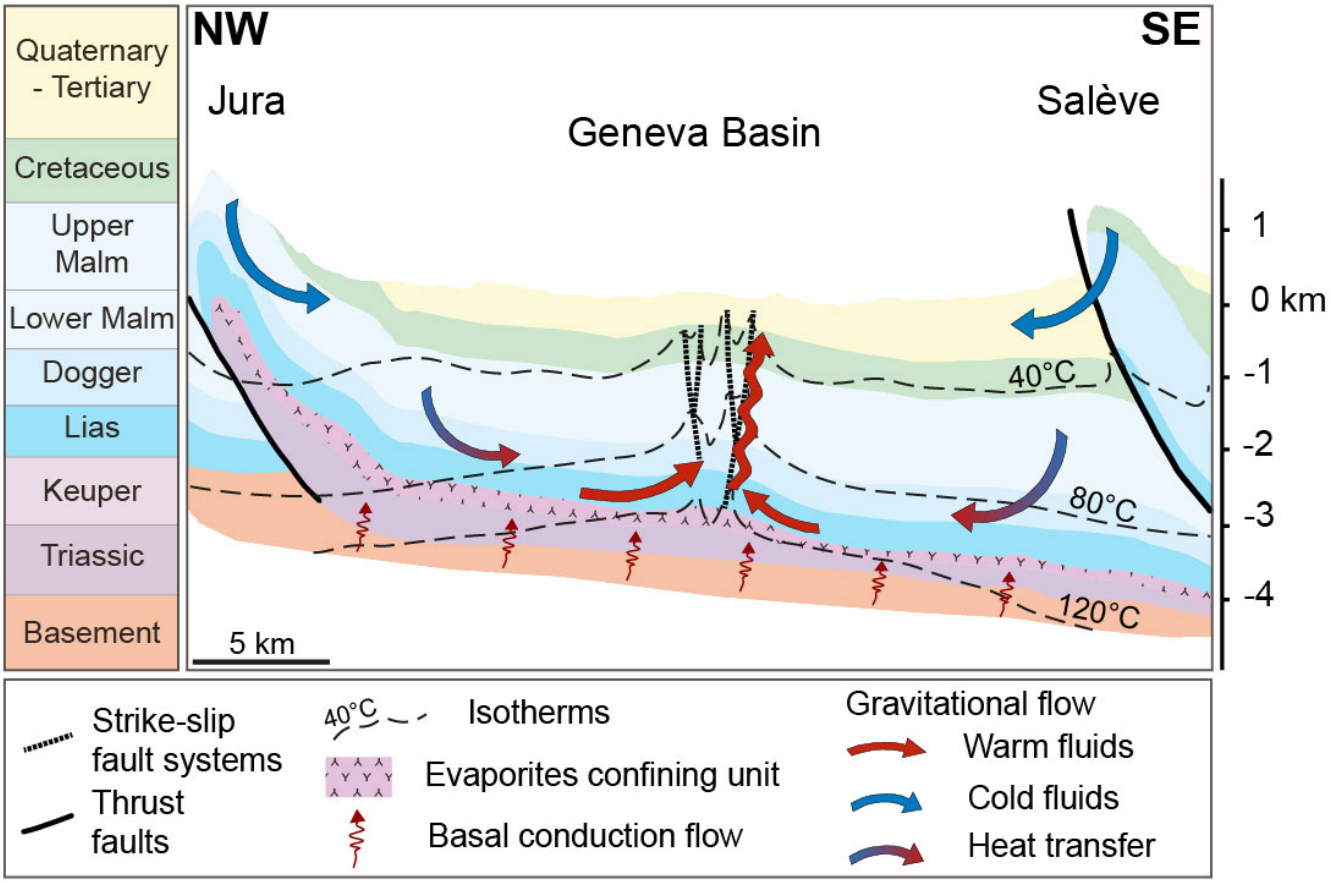

Figure 11. Conceptual fluid flow model of the Geneva Basin driven by gravitational flow. Red arrows: warm fluids. Blue arrows: cold fluid. The assumption made with the blue dashed arrow needs further studies to be confirmed. The lithological layers are the same as in the *Heterogeneous Model*. The isotherms are obtained and interpreted from the *Final Model* cross section XS2, location visible on Figure 3.

6 Conclusions

We developed a 3D fluid flow basin-scale model of the Geneva Basin, France-Switzerland. We suggest that the workflow presented in this study could be more widely applied to other sedimentary basins during the investigation of geothermal systems. In particular, our numerical study was carried out with MRST, (Lie, 2019). We adapted existing libraries and derived a comprehensive workflow that allowed us to use a single tool and design an integrated methodology.

Our study proposes a conceptual groundwater flow model of the Geneva Basin, where fluids are driven by gravitational flow. More precisely, the higher hydraulic head, found below the topographic relieves bordering the basin, drives groundwater circulation. The down-welling fluids cool down the areas at depth on the sides of the basin, while promoting an advective process that focus warmer fluids in the center of the basin where

isotherms bulge. The groundwater flow is separated into two flow regimes by an evaporitic layer that confines cold advecting fluids in the shallow parts of the basin. Preferential flow pathways with high velocities are also observed in the fault zones. Our models suggest that geothermal drilling should take place in the center of the basin.

Acknowledgments

Marion Alcanié is funded by the Swiss National Science Foundation (GENERATE project, PYAPP2 66900, PI Matteo Lupi). Marine Collignon is funded by a Marie Skłodowska-Curie Individual Fellowship (NERUDA 793662). Olav Møyner was funded by VISTA, which is a research program funded by Equinor and conducted in collaboration with The Norwegian Academy of Science and Letters. We would like to thank the SIG (Services Industriels de Genève), HydroGeo Environnement and the actors of the Geothermie 2020 project who provided data and reports. We thank D.Schmid, S. Geiger and one anonymous reviewer for their constructive comments and careful reviews, and the editor C. Facenna for handling our work.

Petrohysical data for this study are included in published data (Capar et al., 2015; Chelle-Michou et al., 2017; Rusillon, 2017) and are extracted from supplementary information files. Compiled tables can be obtained via the link: `http://doi.org/10.5281/zenodo.4541514`. Lithostratigraphic interpreted horizons from the seismic lines by Clerc et al. (2015) used for this research are published data (Allenbach et al., 2017). Reviewers can access the available data through this website [3]. Main code and attached functions to simulate the *Final Model* presented in the study can be found via the link : `http://doi.org/10.5281/zenodo.4541514`.

References

Allenbach, R., Baumberger, R., Kurmann, E., Michael, C. S., & Reynolds, L. (2017). *GeoMol: Modèle géologique 3D du bassin molassique suisse–Rapport Final.* (Tech. Rep.).

Andersson, O. (2007). Aquifer thermal energy storage (ates). In *Thermal energy storage for sustainable energy consumption. nato science series (mathematics, physics and chemistry).* (p. 155-176). Springer.

Antunes, V., Planès, T., Zahradník, J., Obermann, A., Alvizuri, C., Carrier, A., & Lupi, M. (2020). Seismotectonics and 1D velocity model of the Greater Geneva Basin, France-Switzerland. *Geophysical Journal International*, 2026–2047. doi: 10.1093/gji/ggaa129

Baujard, C., Signorelli, S., Kohl, T., & Kommission, S. G. (2007). *Atlas des ressources géothermiques de la suisse occidentale: domaine sud-ouest du plateau suisse.* Commission Suisse de Géophysique.

Bitzer, K., & Carmona, J. M. (2001). Fluid flow processes at basin scale. Procesos de circulación de fluidos a escala de cuenca. *Acta Geologica Hispanica*, *36*, 1–20.

Bonté, D., Limberger, J., Békési, E., Beekman, F., & van Wees, J. D. (2018). Preliminary estimation of the thermal structure of theAcoculco - Los Humeros area, Mexico,. In *uropean geosciencesunion general assembly, egu2018-16270, vienna, austria,2018.*

Breede, K., Dzebisashvili, K., & Liu, X. (2013). A systematic review of enhanced (or engineered) geothermal systems: past, present and future. *Geothermal Energy*, *4*. doi: https://doi.org/10.1186/2195-9706-1-4

Brentini, M. (2018). *Impact d'une donnée géologique hétérogène dans la gestion des géo-ressources: analyse intégrée et valorisation de la stratigraphie à travers le bassin genevois (Suisse, France)* (Doctoral dissertation). doi: 10.13097/archive-ouverte/unige:103409

Burkhard, M., & Sommaruga, A. (1998). Evolution of the western Swiss Molasse basin: structural relations with the Alps and the Jura belt. *Geological Society, London, Special Publications*, *134*, 279–298. doi:

[3] https://ge.ch/sitg/actualites/geomol-donnees-de-base-potentiels-unites-geologiques

10.1144/GSL.SP.1998.134.01.13

Böhm, F., Savvatis, A., Steiner, U., Schneider, M., & Koch, R. (2013). Lithofazielle Reservoircharakterisierung zur geothermischen Nutzung des Malm im Großraum München. *Grundwasser*, *18*, 3—13. doi: 10.1007/s00767-012-0202-4

Capar, L., Couëffé, R., Brenot, A., Courrioux, G., Dezayes, C., Gabalda, S., ... Rusillon, E. (2015). Évaluation des ressources naturelles dans les bassins d'avant-chaîne alpins pour une utilisation et une gestion durable du sous-sol – Zone Pilote Savoie-Genève. *Rapport final, BRGM/RP-64744-FR*, 76.

Cardello, L., Lupi, M., Makhloufi, Y., Do Couto, D., Clerc, N., Sartori, M., ... Meyer, M. (2017). Fault segmentation and fluid flow in the Geneva Basin (France & Switzerland). In *Egu general assembly* (p. p.18673).

Carrier, A., Fischanger, F., Gance, J., Cocchiararo, G., Morelli, G., & Lupi, M. (2019). Deep electrical resistivity tomography for the prospection of low- to medium-enthalpy geothermal resources. *Geophysical Journal International*, *219*, 2056–2072. doi: 10.1093/gji/ggz411

Carrier, A., Nawratil de Bono, C., & Lupi, M. (2020). Affordable gravity prospection calibrated on improved time-to-depth conversion of old seismic profiles for exploration of geothermal resources. *Geothermics*, *86*. doi: 10.1016/j.geothermics.2020.101800

Charollais, J., Weidmann, M., Berger, J. P., Engesser, B., Hotellier, J. F., Gorin, G., ... Schäfer, P. (2007). La Molasse du bassin franco-genevois et son substratum. *Archives des Sciences*, *60*, 59–174.

Charollais, J., Wernli, R., Mastrangelo, B., Metzger, J., Busnardo, R., Clavel, B., ... Weidmann, M. (2013). Présentation d'une nouvelle carte géologique du vuache et du mont de musièges (haute-savoie, france). *Archives des Sciences*, *66*, 1-64.

Chelle-Michou, C., Do Couto, D., Moscariello, A., Renard, P., & Rusillon, E. (2017). Geothermal state of the deep Western Alpine Molasse Basin, France-Switzerland. *Geothermics*, *67*, 48–65. doi: 10.1016/j.geothermics.2017.01.004

Clerc, N., Rusillon, E., Moscariello, A., Renard, P., Paolacci, S., & Meyer, M. (2015). Detailed Structural and Reservoir Rock Typing Characterisation of the Greater Geneva Basin, Switzerland, for Geothermal Resource Assessment. In *Proceedings world geothermal congress, melbourne, australia.* doi: 10.1002/2017EF000724

Collignon, M., Klemetsdal, Ø., Møyner, O., Alcanié, M., Rinaldi, A., Nilsen, H., & Lupi, M. (2020). Evaluating thermal losses and storage capacity in high-temperature aquifer thermal energy storage (HT-ATES) systems with well operating limits: insights from a study-case in the Greater Geneva Basin, Switzerland. *Geothermics*, *85*. doi: 10.1016/j.geothermics.2019.101773

Commission Suisse de Géophysique. (1995). *Geothermal Map of Switzerland 1995 (Heat Flow Density)* (Tech. Rep.). Zurich, Switzerland.

Coumou, D., Matthai, S., Geiger, S., & Driesner, T. (2008). A parallel fe–fv scheme to solve fluid flow in complex geologic media. *Computers Geosciences*, *34*, 1697–1707. doi: 10.1016/j.cageo.2007.11.010

Diersch, H.-J. G. (2013). *Feflow: finite element modeling of flow, mass and heat transport in porous and fractured media*. Springer Science & Business Media.

Dragon, K. (2008). The influence of anthropogenic contamination on the groundwater chemistry of a semi-confined aquifer (the wielkopolska buried valley aquifer, poland). *Water Resource Management*, *22*, 343-355. doi: https://doi.org/10.1007/s11269-007-9165-0

Driesner, T. (2007). The system H_2O-NaCl II. correlations for molar volume, enthalpy, and isobaric heat capacity from 0 to 1000 degrees C, 1 to 5000 bar, and 0 to 1 X_{NaCl}. *Geochimica et Cosmochimica Acta*, *71*, 4902–4919.

Duddy, I. R., Green, P. F., Bray, R. J., & Hegarty, K. A. (1994). Recognition of the thermal effects of fluid in sedimentary basins. *Geofluids: origin, migration and evolution of fluids in sedimentary basins*(78), 325–345. doi: 10.1016/0148-9062(95)94526-1

Dupuy, D. (2006). *Étude des sédiments quaternaires, de la molasse et sa tectonique, dans le Grand Lac (Léman) à partir de données sismiques 2D et 3D* (Unpublished doctoral dissertation). University of Lausanne.

Eruteya, O.-E., Guglielmetti, L., Makhloufi, Y., & Moscariello, A. (2019). 3-D Static Model to Characterize Geothermal Reservoirs for High-Temperature Aquifer Thermal Energy Storage (HT-ATES) in the Geneva Area, Switzerland. In *Sccer-soe annual conference 2019* (p. poster). doi: 10.13140/RG.2.2.23299.45606

Faessler, J., Lachal, B. M., Quiquerez, L., & de Genève, S. S. I. (2015). *Géothermie de moyenne profondeur: Scénarios d'utilisation de la ressource via des réseaux de chauffage à distance - enjeux et principaux enseignements.* Genève: Services Industriels de Genève.

Garibaldi, C., Guillou-frottier, L., Lardeaux, J.-m., Bouchot, V., Guillemin, A. C., Azur, G., ... Antipolis, S. (2010). Combination of Numerical Tools to Link Deep Temperatures , Geological Structures and Fluid Flow in Sedimentary Basins : Application to the Thermal Anomalies of the Provence Basin (South-East France). In *World geothermal congress 2010.*

Glassley, E. W. (2014). *Geothermal Energy: Renewable Energy and the Environment, Second Edition.* CRC Press, Taylor and Francis Group.

Gorin, G., Signer, C., & Amberger, G. (1993). Structural configuration of the western Swiss Molasse Basin as defined by reflection seismic data. *Eclogae Geologicae Helvetiae*, *86*, 693–716.

Guglielmetti, L., Perozzi, L., Dupuy, D., Martin, F., Métraux, V., Meyer, M., ... Moscariello, A. (2020). High Resolution Gravity Data to Characterize Density Variations and Reduce Uncertainty in Geothermal Reservoirs in the Geneva Basin(GB)..

Guillou-Frottier, L., Carre, C., Bourgine, B., Bouchot, V., & Genter, A. (2013). Structure of hydrothermal convection in the Upper Rhine Graben as inferred from corrected temperature data and basin-scale numerical models. *Journal of Volcanology and Geothermal Research*, *256*, 29–49. doi: 10.1016/j.jvolgeores.2013.02.008

Guillou-Frottier, L., Duwiquet, H., Launay, G., Taillefer, A., Roche, V., & Link, G. (2020). On the morphology and amplitude of 2D and 3D thermal anomalies induced by buoyancy-driven flow within and around fault zones. *Solid Earth*, *11*, 1571–1595. doi: 10.5194/se-11-1571-2020

Hairuo Qing, & Mountjoy, E. (1992). Large-scale fluid flow in the Middle Devonian Presqu'ile barrier, western Canada sedimentary basin. *Geology*, *20*, 903–906. doi: 10.1130/0091-7613(1992)020<0903:LSFFIT>2.3.CO;2

Hamm, V., & Treil, J. (2013). *Gestion de la base de données du Dogger en Île-de-France* (Tech. Rep.). BRGM. Technical Report.

Homewood, P., Allen, P. A., & Williams, G. D. (1986). Dynamics of the Molasse Basin of Western Switzerland. *Foreland Basins special publications*, *8*, 199–217.

Housse, B., & Maget, P. (1976). *Potentiel Geothermique du Bassin Parisien* (Tech. Rep.). Elf Aquitaine and BRGM.

Ingebritsen, S., & Manning, C. (2010). Permeability of the continental crust: Dynamic variations inferred from seismicity and metamorphism. *Geofluids*, *10*, 193–205. doi: 10.1111/j.1468-8123.2010.00278.x

Jasechko, S., Perrone, D., & Befus, K. (2017). Global aquifers dominated by fossil groundwaters but wells vulnerable to modern contamination. *Nature Geoscience*, *10*, 425—429. doi: https://doi.org/10.1038/ngeo2943

Jialing, Z., Kaiyong, H., Xinli, L., Xiaoxue, H., Ketao, L., & Xiujie, W. (2015). A review of geothermal energy resources, development, and applications in china: Current status and prospects. *Energy*, *93*, 466–483. doi: https://doi.org/10.1016/j.energy.2015.08.098

Joukowsky, E. (1941). *Géologie et eaux souterraines du pays de Genève.* Geneva: Kundig.

Kipp, K., Hsieh, P., & Charlton, S. (2008). *Guide to the Revised Ground-Water Flow and Heat Transport Simulator: HYDROTHERM – Version 3* (Tech. Rep.).

Krogstad, S., Lie, K. A., Møyner, O., Nilsen, H. M., Raynaud, X., & Skaflestad, B. (2015). MRST-AD - An open-source framework for rapid prototyping and evaluation of reservoir simulation problems. In *Spe reservoir simulation symposium 2015, 23–25 february, houston, texas.* doi: 10.2118/173317-MS

Kulcar, B., Goricane, D., & Krope, J. (2008). Economy of exploiting heat from low-temperature geothermal sources using a heat pump. *Energy and Buildings*, *40*, 323–329. doi: 10.1016/j.enbuild.2007.02.033

Lavigne, J., & Maget, P. (1977). *Les ressources geothermiques francaises : possibilites de mise en valeur* (Tech. Rep.). BRGM.

Lie, K.-A. (2019). *An Introduction To Reservoir Simulation Using Matlab/GNU Octave : User guide for the Matlab Reservoir Simulation Toolbox (MRST).* Cambridge University Press.

Lopez, S., Hamm, V., Le Brun, M., Schaper, L., Boissier, F., Cotiche, C., & Giuglaris, E. (2010). 40 years of Dogger aquifer management in Ile-de-France, Paris Basin, France. *Geothermics*, *39*, 339–356.

Luijendijk, E., Winter, T., Köhler, S., Ferguso, G., Von Hagke, C., & Scibek, J. (2020). Using thermal springs to quantify deep groundwater flow and its thermal footprint in the Alps and North American orogens. *Geophysical Research letters.* doi: 10.31223/osf.io/364dj

Lupi, M., Geiger, S., & Graham, C. (2010). Hydrothermal fluid flow within a tectonically active rift-ridge transform junction: Tjörnes Fracture Zone, Iceland. *Journal of Geophysical Research*, *115*. doi: https://doi.org/10.1029/2009JB006640

Makhloufi, Y., Rusillon, E., Brentini, M., Moscariello, A., Meyer, M., & Samankassou, E. (2018). Dolomitization of the upper jurassic carbonate rocks in the geneva basin, switzerland and france. *Swiss Journal of Geosciences.*

Manning, C., & Ingebritsen, S. (1999). Permeability of the continental crust: Implications of geothermal data and metamorphic systems. *Review of Geophysics*, *37*, 127–150. doi: 10.1029/1998RG900002

Matthai, S., Geiger, S., Roberts, S., Paluszny, A., Belayneh, M., Burri, A., ... Heinrich, C. (2007). Numerical simulation of multi-phase fluid flow in structurally complex reservoirs. *Geological Society London Special Publications*, *292*, 405-429. doi: 10.1144/SP292.22

Mays, L. (2013). Groundwater resources sustainability: Past, present, and future. *Water Resource Management*, *27*, 4409–4424. doi: https://doi.org/10.1007/s11269-013-0436-7

Menjoz, A., Azaroual, M., Sbai, A., & Ungemach, P. (2004). Mise en œuvre d'un système de gestion de la ressource géothermique du dogger de la région he-de-france phase rp-52927-fr.

Montegrossi, G., Deb, P., Clauser, C., Diez, H., & Ramirez Montes, M. (2018). Modeling of Los Humeros geothermal field: preliminary results. In *20th egu general assembly, egu2018, proceedings from the conference 2018 in vienna, p.17600.*

Moscariello, A. (2019). Exploring for geo-energy resources in the geneva basin (Western Switzerland): Opportunities and challenges. *Swiss Bulletin for Applied Geology*, *24*, 105–124.

Nilsen, H. M., Lie, K.-A., & Natvig, J. R. (2012). Accurate modelling of faults by multipoint, mimetic, and mixed methods. *SPE Journal*, *17*, 56_–579. doi: 10.2118/149690-PA

Nowak, K. (2011). *Renewable energy potential and its exploitation on a regional scale* (Unpublished).

Olasolo, M., Juárez, M., Morales, S., & Liarte, I. (2016). Enhanced geothermal systems (EGS): A review. *Renewable and Sustainable Energy Reviews*, *56*, 133–144. doi: 10.1016/j.rser.2015.11.031

Paolacci, S. (2012). *Seismic facies and structural configuration of the western alpine molasse basin and its substratum (france and switzerland)* (Unpublished doctoral dissertation).

Person, M., Raffensperger, J., Ge, S., & Garven, G. (1996). Basin-scale hydrogeologic modeling. *Review of Geophysics*, *34*, 61–87. doi: 10.1029/95RG03286

Planès, T., Obermann, A., Antunes, V., & Lupi, M. (2020). Ambient-noise tomography of the Greater Geneva Basin in a geothermal exploration context. *Geophysical Journal International*, *220*, 370–383. doi: 10.1093/gji/ggz457

Pruess, K., Oldenburg, C., & Moridis, G. (2012). *TOUGH2 User's Guide* (Tech. Rep.).

Przybycin, A. M. (2015). *Lithospheric-scale 3D structural and thermal modelling and the assessment of the origin of thermal anomalies in the European North Alpine Foreland Basin* (Unpublished doctoral dissertation).

Przybycin, A. M., Scheck-Wenderoth, M., & Schneider, M. (2017). The origin of deep geothermal anomalies in the German Molasse Basin: results from 3D numerical models of coupled fluid flow and heat transport. *Geothermal Energy*, *5*, 1–28. doi: 10.1186/s40517-016-0059-3

Ramsay, J. G. (1963). Stratigraphy, structure and metamorphism in the western alps. *Proceedings of the Geologists' Association*, *74*, 357-390.

Rusillon, E. (2017). *Characterisation and rock typing of deep geothermal reservoirs in the Greater Geneva Basin (Switzerland & France)* (Doctoral dissertation). doi: 10.13097/archive-ouverte/unige:105286

Rybach, L. (1992). Geothermal potential of the Swiss Molasse Basin. *Eclogae Geologicae Helvetiae*, *85*, 733–744.

Schärli, U., & Rybach, L. (2001). Determination of specific heat capacity on rock fragments. *Geothermics*, *30*, 93–110. doi: 10.1016/S0375-6505(00)00035-3

Sharqawy, M. H. (2013). New correlations for seawater and pure water thermal conductivity at different temperatures and salinities. *Desalination*, *313*, 97–104. doi: 10.1016/j.desal.2012.12.010

Shemin Ge, & Garven, G. (1992). Hydromechanical modeling of tectonically driven groundwater flow with application to the Arkoma foreland basin. *Journal of Geophysical Research*, *97*, 9119–9144. doi: 10.1029/92jb00677

Sibson, R. (1996). Structural permeability of fluid-driven fault-fracture meshes. *Journal of Structural Geology*, *8*, 1031–1042. doi: 10.1016/0191-8141(96)00032-6

Signer, C., & Gorin, G. (1995). New geological observations between the Jura and the Alps in the Geneva area, as derived from reflection seismic data. *Eclogae Geologicae Helvetiae*, *88*, 235–265.

Sommaruga, A. (1997). *Geology of the central jura and the molasse basin: new insight into an evaporite-based foreland fold and thrust belt* (Unpublished doctoral dissertation).

Sommaruga, A. (1999). Décollement tectonics in the jura foreland fold-and-thrust belt. *Marine and Petroleum Geology*, *16*, 111-134.

Sommaruga, A., Eichenberger, U., & Marillier, F. (2012). *Seismic Atlas of the Molasse Basin* (Tech. Rep.).

Spivey, J., W.D., M., & North, R. (2004). Estimating Density, Formation Volume Factor, Compressibility, Methane Solubility, and Viscosity for Oilfield Brines at Temperatures From 0 to 275 ° C, Pressures to 200 MPa, and Salinities to 5.7 mole/kg. *Journal of Canadian Petroleum Technology*, *10*. doi: https://doi.org/10.2118/04-07-05

Sweetkind, D., Masbruch, M., Heilweil, V., & Buto, S. (2010). *Groundwater Flow* (Tech. Rep.).

Taillefer, A., Guillou-Frottier, L., Soliva, R., Magri, F., Lopez, S., Courrioux, G., ... Le Goff, E. (2018). Topographic and Faults Control of Hydrothermal Circulation Along Dormant Faults in an Orogen. *Geochemistry, Geophysics, Geosystems*, *19*, 4972–4995. doi: 10.1029/2018GC007965

The GeoMol Team. (2015). *GeoMol – Assessing subsurface potentials of the Alpine Foreland Basins for sustainable planning and use of natural resources* (Tech. Rep.).

Trefry, M. G., & Muffels, C. (2007). Feflow: A finite-element ground water flow and transport modeling tool. *Groundwater*, *45*(5), 525–528.

Trümpy, R. (1980). *Geology of switzerland - a guide-book. part a: An outline of the geology of switzerland. part b: Geological excursions.* Wepf and Co.

Velis, M., Conti, K., & Biermann, F. (2017). Groundwater and human development: synergies and tradeoffs within the context of the sustainable development goals. *Sustainable Science*, *12*, 1007–1017. doi: https://doi.org/10.1007/s11625-017-0490-9

Waples, D. W., & Waples, J. S. (2004). A review and evaluation of specific heat capacities of rocks, minerals, and subsurface fluids. Part 2: Fluids and porous rocks. *Natural Resources Research*, *13*, 123–130. doi: 10.1023/B:NARR.0000032648.15016.49